

Study of the determination of the SUGRA parameters using the ATLAS detector in the case of L -violating R parity breaking

Adrian MIREA and Elemér NAGY

*Centre de Physique des Particules de Marseille,
Faculté des Sciences de Luminy,
IN2P3-CNRS, F-91288 Marseille, CEDEX 09 France*

ATL-PHYS-99-007
21/04/99



Abstract

Simulating pp collisions at LHC energies in the framework of the SUGRA model and the detection of the produced leptons and jets by ATLAS we demonstrate that a clean signature of SUSY can be obtained over a large domain of the parameter space in the case of L -violating R parity breaking (λ couplings). The obtained signal allows the reconstruction of the SUSY particles and thereby the precise determination of the model parameters m_0 , $m_{1/2}$, $\tan\beta$ and $\text{sign}\mu$.

1 Introduction

The ATLAS Collaboration has carried out a detailed study to detect the SUSY signature in the framework of one of the most popular model, SUGRA [1],[2]. It has been shown [3] that if SUSY exists at the electro-weak scale, it should be discovered by ATLAS and a general method has been given to determine approximately the mass scale of the SUSY particles. In subsequent papers [4]–[7] it was shown in five representative points of the parameter space that some of the SUSY particles can be reconstructed and using the obtained characteristics (masses, branching ratios) the model parameters can be precisely determined [8]. All these studies have been carried out assuming that R parity is conserved.

In this note we consider that R parity is broken in such a way that the lepton number L is violated through λ -type couplings. The present experimental limits [9] cannot completely exclude such a scenario. In this case one of the prominent signatures of SUSY, the missing energy is considerably weakened because the lightest SUSY particle (LSP) is allowed to decay. Due to this decay the lepton and/or jet multiplicity increases considerably and some efficient cuts (e.g. lepton veto against the $t - \bar{t}$ background) cannot be applied. On the other hand, the decay products of the LSP in some cases allow its direct reconstruction. Therefore the event topology and the search strategies are different of the case when R is conserved. This has motivated us to revisit the feasibility to detect SUSY and to determine the parameters of the SUGRA model using the ATLAS detector.

In section 2 we give a brief description of the phenomenology of the R parity violation and the event generator used. Section 3 deals with the ATLAS detector and with the fast simulation of its response. In section 4 we present the domain of the parameter space where a SUSY signal can be expected by ATLAS. In the subsequent three sections the reconstruction of the SUSY particles and the determination of the model parameters are described in the LHC points 1,3 and 5 which represent a heavy, light and medium SUSY mass scale. We summarize the obtained results in the concluding section.

2 Basic Phenomenology

2.1 R parity violation

R -parity has been introduced [10] in order to avoid fast nucleon decay and flavor changing neutral currents (FCNC). If the multiplicative quantum number

$$R = (-1)^{3B+L+2S} \quad (1)$$

is conserved it guarantees automatically baryon number (B) and lepton number (L) conservation. R is +1 for Standard Model (SM) particles and its value is -1 for their superpartners. The most important experimental consequences of the conservation of R are that super partners should be produced in pairs and the lightest superpartner (LSP) should be stable. The LSP interacts weakly, therefore the prominent signature of SUSY in case of R parity conservation is a considerable amount of missing (transverse) energy (E_T^{miss}).

Although no violation of B or L has been observed yet, there is no firm theoretical argument which would require exact conservation of them and that of the R parity. In fact the following term in the superpotential

$$W_{\mathcal{R}} = \lambda_{ijk} L_i L_j E_k^c + \lambda'_{ijk} Q_i L_j D_k^c + \lambda''_{ijk} U_i^c D_j^c D_k^c \quad (2)$$

which violates explicitly B , L and R parity, cannot be ruled out experimentally. Here L and E are isodoublet and isosinglet lepton, Q and D are isodoublet and isosinglet quark superfields, the indices i , j and k run for the three lepton and quark families. The suffix c denotes charge conjugate. The first two terms violate explicitly L whilst the last one violates B . Present limits on the proton lifetime suggests that either the L or the B violating terms (i.e. the corresponding λ_{ijk} couplings) should vanish for the first family. Other experimental limits e.g. on lepton number violation: double β decay, or on $N - \bar{N}$ oscillation, etc. indicate that the couplings in Equ. (2) shouldn't be expected to exceed a few percent, and usually are much smaller than the gauge couplings. Even so, if R parity is violated the topology of the expected SUSY signal changes substantially. Since the LSP is no more stable, the missing energy is considerably reduced. On the other hand the decay products of the LSP increase the average number of jets and/or leptons in an event. In general, the event topology depends crucially on the size of the couplings. If, e.g. the couplings are of the order of $\sim 10^{-2}$ or larger, the mass spectra, branching ratios, etc. will be different in the two cases where R is conserved or violated. If however the couplings are smaller than the above value, the dominant effect of the R parity violation is that the LSP becomes unstable. An estimation of the LSP lifetime as a function of the couplings

show [11] that we can distinguish four subcases giving rise to different detection strategies:

- (i) $10^{-4} \leq \lambda \leq 10^{-2}$
- (ii) $10^{-6} \leq \lambda \leq 10^{-4}$
- (iii) $10^{-9} \leq \lambda \leq 10^{-6}$
- (iv) $\lambda \leq 10^{-9}$

In case (i) only the event topology changes w.r.t. the case of R conservation. In case (ii) one can observe a displaced vertex at the LHC energies. In case (iii) the LSP decays outside of a typical LHC detector, however it can be caught by special purpose detectors [12]. Finally the case (iv) cannot be distinguished experimentally from the case of R parity conservation.

In this study we have deliberately chosen to study case (i) and compare the result with the case of R parity conservation, because it represents a more difficult experimental situation than case (ii) where a displaced vertex could disentangle the LSP from the rest of the event. Moreover we have assumed that $\lambda'_{ijk} = \lambda''_{ijk} = 0$ and only one of the λ_{ijk} coupling is different from zero in Equ. (2). Nonzero λ'_{ijk} and λ''_{ijk} are subject of other reports inside ATLAS [16]. The hierarchical structure observed for the Yukawa couplings in the SM motivates our hypothesis above. The Lagrangian corresponding to the superpotential of Equ. (2) can be written in terms of particle fields for our case as:

$$L_{\mathcal{W}}^{\lambda} = \frac{1}{2} \lambda_{ijk} (\bar{\nu}_{L_i}^c e_{L_j} \tilde{e}_{R_k}^* - e_{L_i} \bar{\nu}_{L_j}^c \tilde{e}_{R_k}^* + \nu_{L_i} \tilde{e}_{L_j} \bar{e}_{R_k} - e_{L_i} \tilde{\nu}_{L_j} \bar{e}_{R_k} + \tilde{\nu}_{L_i} e_{L_j} \bar{e}_{R_k} - \tilde{e}_{L_i} \nu_{L_j} \bar{e}_{R_k}) + HC \quad (3)$$

where ν_L and $e_{L,R}$ are lepton fields, the tilde denotes the field of the superpartner, the c stands for charge conjugation, $*$ for complex conjugation and i, j, k are the flavor indices. As stated before, if the λ couplings are smaller than 10^{-2} , which is our case, the sparticle mass spectrum practically doesn't change and the main consequence of the R parity violation is the decay of the LSP. This process is depicted in Fig.1 where we assume that the LSP is the lightest neutralino ($\tilde{\chi}_1^0$). The decay proceeds through an R conserving and an R violating vertex and in the final state there are always three leptons out of them at least two of *different* flavours, one neutral and the other two of opposite charges, since the LSP is supposed to be neutral.

The prominent signature of this type of SUSY event is the spectacular increase of "stable" leptons: electrons and muons in the final state. The neutral leptons, neutrinos, give rise to some missing transverse energy, but its magnitude is much less than that if R parity is conserved. The flavour of the lepton in the final state depends on the values of the indices i, j, k . Since λ_{ijk} is antisymmetric in i and j there are only 9 independent couplings which we choose as: $\lambda_{121}, \lambda_{122}, \lambda_{123}, \lambda_{131}, \lambda_{132}, \lambda_{133}, \lambda_{231}, \lambda_{232}, \lambda_{233}$. The first two families, 1 and 2 give rise always to "stable" leptons, electrons and muons, (and the corresponding neutrinos) in the final state. If an index 3 appears, the lepton is not stable if it is a τ , and its decay products are most of the time different from electrons or muons. Since e in Equ. (2) is an isosinglet, e_3 is a τ . The number of the stable leptons is the most prominent for λ_{121} and λ_{122} . It is less spectacular, if an index 3 appears at the second place, and even less if the 3 appears in the third place. Finally, if two indices have value of 3 one has the least number of stable leptons. On the other hand, the number of the neutrinos, and with that the magnitude of the missing energy increases in the order of the above mentioned cases. The expected extra number of stable charged leptons and neutrinos per each LSP decay for the different λ couplings calculated by the program [13] are given in Table 1. It is clear that the average number of the leptons for different flavours gives a strong hint on

the coupling which is realized. E.g. the coupling λ_{122} gives rise predominantly to muons whilst the coupling λ_{123} results in equal number of electrons and muons, etc.

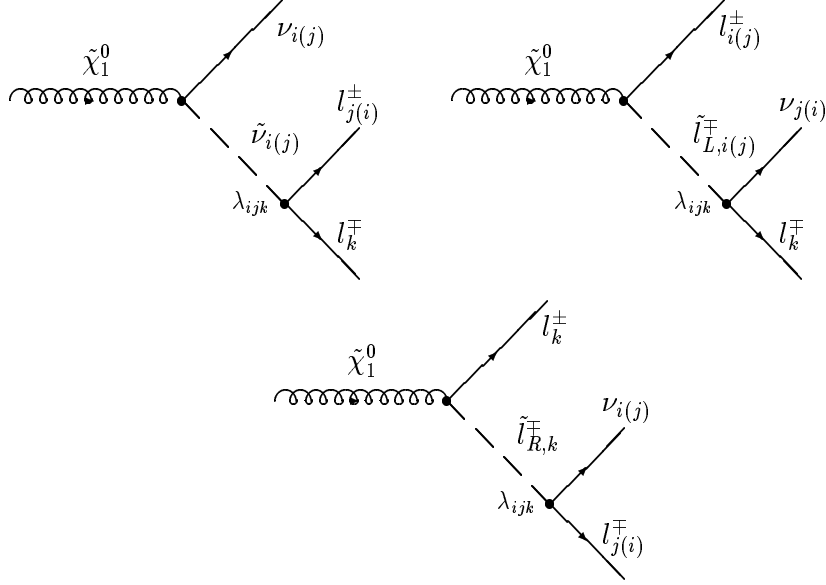


Figure 1: The R decays of $\tilde{\chi}_1^0$ (assumed as LSP) through λ type couplings.

Table 1: The number of produced stable leptons in the LSP decay if it is the $\tilde{\chi}_1^0$. We have assumed $\sim 18\%$ branching ratio for the semileptonic decay of the τ .

λ_{ijk}	Decay channel	$\langle N_e \rangle$	$\langle N_\mu \rangle$	$\langle N_\nu \rangle$
121	$e^\pm \nu_\mu e^\mp; \nu_e \mu^\pm e^\mp$	1.5	0.5	1
122	$e^\pm \nu_\mu \mu^\mp; \nu_e \mu^\pm \mu^\mp$	0.5	1.5	1
123	$e^\pm \nu_\mu \tau^\mp; \nu_e \mu^\pm \tau^\mp$	0.68	0.68	2.36
131	$e^\pm \nu_\tau e^\mp; \nu_e \tau^\pm e^\mp$	1.59	0.09	1.68
132	$e^\pm \nu_\tau \mu^\mp; \nu_e \tau^\pm \mu^\mp$	0.59	1.09	1.68
133	$e^\pm \nu_\tau \tau^\mp; \nu_e \tau^\pm \tau^\mp$	0.77	0.27	3.04
231	$\mu^\pm \nu_\tau e^\mp; \nu_\mu \tau^\pm e^\mp$	1.09	0.59	1.68
232	$\mu^\pm \nu_\tau \mu^\mp; \nu_\mu \tau^\pm \mu^\mp$	0.09	1.59	1.68
233	$\mu^\pm \nu_\tau \tau^\mp; \nu_\mu \tau^\pm \tau^\mp$	0.27	0.77	3.04

The presence or absence of τ 's influence how easily the SUSY particles can be reconstructed. On the one hand the signature is weakened by the taus since they produce less stable charged leptons, and these, partly originating from the τ decay, do not produce a sharp endpoint for the $\tilde{\chi}_1^0$ mass. On the other hand, taus produce more missing transverse energy, moreover the smaller number of stable charged leptons produced decreases the combinatorial background in the mass reconstruction.

2.2 The SUGRA Model

The present study of R parity violation is carried out in the framework of the SUGRA model [1],[2]. Contrary to the minimal version of supersymmetric models (MSSM) which has a very large number of unknown parameters, the SUGRA model is characterized only by 5 parameters which are the following:

- (1) m_0 , an universal scalar mass,
- (2) $m_{1/2}$, an universal gaugino mass,
- (3) A_0 a common trilinear interaction term,
- (4) $\tan(\beta)$, the ratio of the vacuum expectation values of the two Higgs fields,
- (5) the sign of μ of the Higgsino mass parameter.

The mass spectrum of the SUSY partners at the electro-weak scale as well as their decay branching ratios are obtained from the above parameters by solving the renormalization group equations (RGE). This is performed in our case by the program of ISAJET [14].

The SUGRA model predicts a hierarchical structure of the masses of the SUSY particles. The masses of the first two families of the squarks and of the sleptons are driven essentially by m_0 and $m_{1/2}$ through an approximate relation :

$$m_{\tilde{f}_{L,R}}^2 = m_0^2 + m_f^2 + c(\tilde{f}_{L,R}) \cdot m_{1/2}^2 + D(\tilde{f}_{L,R}) \quad (4)$$

where $c(\tilde{f})$ are some numerical factors of order $5.5 \div 6.0$ for the squarks and of order $0.15 \div 0.5$ for the sleptons, $D(\tilde{f}_{L,R})$ are the so-called D-terms (in general less important). For the third family of the squarks and the sleptons there is a mixing due to the corresponding Yukawa couplings, pushing down the mass of one of the sfermions and the other one in the opposite direction. In some regions of the parameter space this could have the effect that the lighter stau ($\tilde{\tau}_1$) could become the LSP but such scenarios are ruled out by cosmological considerations. The gauginos $U(1)$, $SU(2)$ and $SU(3)$ are driven mainly by $m_{1/2}$. Because the $U(1)$ and $SU(2)$ gauginos will mix with higgsinos to obtain the mass states ($\tilde{\chi}_i^0$, $i = 1, 4$, and $\tilde{\chi}_j^\pm$, $j = 1, 2$), part of that spectrum will depend on the μ parameter (in SUGRA μ is determined by the condition of electro-weak symmetry breaking and typically $\mu \gg m_{1/2}$). We have the following approximate relations:

$$\begin{aligned} m_{\tilde{g}} &\approx 2.4 \cdot m_{1/2} \\ m_{\tilde{\chi}_1^0} &\approx 0.4 \cdot m_{1/2} \\ m_{\tilde{\chi}_2^0} &\approx m_{\tilde{\chi}_1^\pm} \approx 0.8 \cdot m_{1/2} \\ m_{\tilde{\chi}_3^0} &\approx m_{\tilde{\chi}_4^0} \approx m_{\tilde{\chi}_2^\pm} \approx |\mu| \end{aligned} \quad (5)$$

The Higgs sector is composed in SUGRA by five mass states (h^0 , A^0 , H^0 and H^\pm). In the case of the lightest one, $m_{h^0} \leq 130 \div 150$ GeV in about all SUGRA parameter space. The masses of the other Higgses are in general very heavy and depend on $\tan(\beta)$.

The gaugino-higgsino mixing depends more strongly on the parameter values, and this in turn determines the decay branching ratios.

3 The analysis chain

3.1 The event generators

Simulation of the signal events

Our basic program tool is ISAJET¹ [14] which simulates for hadron colliders the production and decay of the supersymmetric particles, as well as the underlying event, i.e. the accompanying partons and their hadronization.

ISAJET does not include R parity violation in the SUGRA model. It has been introduced in detail in another event generator, SUSYGEN [18], written for e^+e^- collisions. Therefore, inspired by SUSYGEN, a set of routines computing in detail all the R (λ -type) decays of gauginos ($\tilde{\chi}_i^0$, $i = 1, 4$ and $\tilde{\chi}_j^\pm$, $j = 1, 2$) and sleptons was written for ISAJET [13]. This program is able to simulate production of supersymmetric particles in a hadronic collision with R parity broken, if this latter is accompanied by L number violation. To obtain correct predictions, the hypothesis of small values of the λ couplings ($\lambda \leq 10^{-2}$) must be used, which is our present case, in order to neglect any correction in the sparticle mass spectrum brought by RGE's. The dominant effect of the R parity violation is the decay of the LSP.

We have generated several million signal events. In Table 2 one can see their repartition in the SUGRA parameter space and for the type of the couplings. In the last column we quote the integrated luminosity in terms of LHC months the generated events correspond to where we have taken an LHC year equivalent to 10^4 /pb (low lumonosity run with appr. 1/3 of efficiency).

Table 2: The number of generated signal events

m_0 [GeV]	$m_{1/2}$ [GeV]	A_0	$\tan(\beta)$	$\text{sgn}(\mu)$	coupling	Events	LHC month
0 - 1500	0 - 1500	0	2	+1	λ_{123}	256 000	—
0 - 500	0 - 500	0	2	+1	λ_{123}	300 000	—
400	400	0	2	+1	λ_{122}	400 000	~ 36
					λ_{123}	400 000	~ 36
200	100	0	2	-1	λ_{123}	1 000 000	~ 1.5
					λ_{122}	1 000 000	~ 1.5
100	300	300	2.1	+1	λ_{123}	450 000	~ 36
					λ_{122}	450 000	~ 36

The samples in the first two rows were used to study inclusive reactions. The rest of the statistics is devoted to the 1st, 3rd and 5th of the so called LHC points, where the determination of the SUGRA parameters has been performed.

Simulation of the background events

As mentioned, the signature of the signal events is the appearance of a large number of high p_t leptons accompanied by high p_t jets and by a moderate amount of missing transverse energy. Such event topology is also produced, albeit in a much reduced level, by the decay of heavy SM particles and these events constitute the main background. We have studied such processes using the ISAJET and PYTHIA [19] event generators

¹We have used version 7.30

including initial and final state radiation. The background event statistics is listed in Table 3.

Table 3: The number of generated background events

Reaction	Number of events
$t - \bar{t}$	1 200 000
$W - Z, W - W$ and $Z - Z$	600 000
$Z - b\bar{b}$	600 000
Drell-Yan	600 000

3.2 Fast simulation of the ATLAS detector

Due to the large number of events to be generated the detector response could not have been simulated in detail, using e.g. GEANT [20]. Instead a fast, so called particle level Monte Carlo program, ATLFAST [15] has been used². In this program the ATLAS detector [21] is described by a simplified geometry and apart of the acceptance the detector response is parametrized. Below we repeat the main features of these description.

Description of ATLAS by ATLFAST

The detector geometry is given in the variables of the pseudorapidity $\eta = -\ln \tan(\theta/2)$ and azimuthal angle ϕ , where θ is the solid angle of the particle produced in the interaction point. The granularity in $\eta \times \phi$ is 0.1×0.1 for $|\eta| < 3$ and 0.2×0.2 otherwise upto $|\eta| = 5$. The produced particles except the muons and the neutrinos deposit their energies, smeared by a resolution function, and are integrated in individual η - ϕ cells. The effect of the 2T solenoidal magnetic field on the deposited energy of the charged particles is parametrized. The effect of cracks in the calorimeter and in the trackers are taken into account by the parametrized acceptance function.

Reconstruction algorithms

First clusters are created from the cell energies using a simple algorithm. Next, isolated photons and electrons are reconstructed if the simulated particle falls in the acceptance region (typically $|\eta| < 2.5$), its energy, smeared by a parametrized resolution function, matches that of a cluster, and in the case of electrons, the η and ϕ values of the cluster and the electron are the same within the resolution. The energy of the reconstructed particles is that of the simulated one smeared by a parametrized resolution, whereas their direction stays the same.

After having removed the clusters of the isolated photons and electrons the reconstruction of the parton jets is carried out by a simple fixed cone algorithm. Isolation criteria of jets or charged tracks can be defined as a function of the deposited energy in a $\Delta R = \sqrt{(\Delta\eta)^2 + (\Delta\phi)^2}$ cone. The reconstructed jet energy in general doesn't match with the true energy of the corresponding parton. Therefore a correction factor has to be applied in a later phase of the analysis. This correction factor, depending on the cone size and on the momentum of the jet, is established by comparing the reconstructed jet transverse momentum with that of the original parton: $R_{calib}^{bjet} = p_t^{bparton} / p_t^{bjet}$. It has been demonstrated that applying such factors one can correctly reconstruct the position of the mass peak of the Higgs boson [15]. This correction factor depends on the jet type and also

²We have used the version 1.57

if the jet contains prompt leptons. In Fig.2 the correction is shown for the three different LHC points analysed. The observed difference in point 3 and the other two points is due to the facts that :

(i) the production mechanisms of the b 's are different. In point 1 and 5 they originate mainly from the decay $h^0 \rightarrow b\bar{b}$, whereas in point 3 the production of the b 's is less correlated;

(ii) in point 3 there are more leptons produced and therefore the probability is higher that a lepton is inside the jet-cone.

One has to stress that the dispersion of the correction factor can be rather large, reaching even 25%, especially at low p_t (≤ 100 GeV). Fig.3 shows the invariant mass of the $b\bar{b}$ pair from the h^0 mass at the LHC points 1 and 5 after having applied the correction.

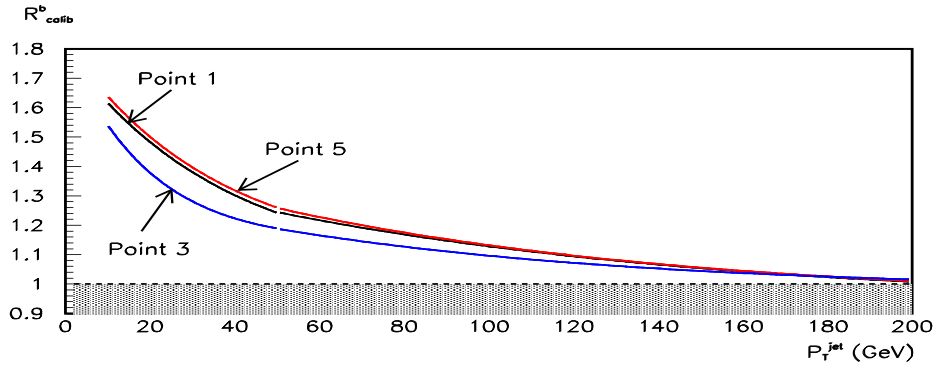


Figure 2: Calibration functions of b jets for SUGRA points 1, 3 and 5.

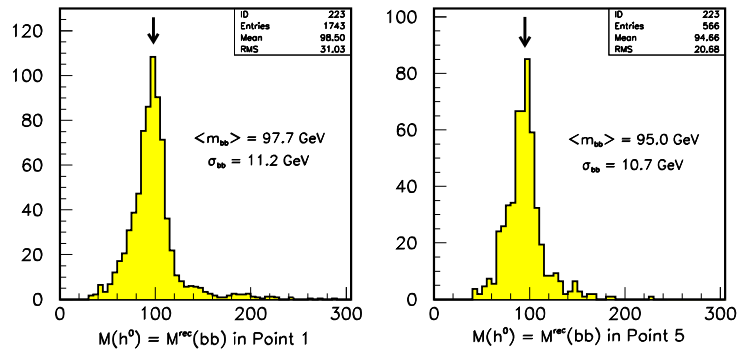


Figure 3: The effect of the resolution and calibration of b jets on the invariant mass distributions in SUGRA points 1 (left) and 5 (right) and for the \mathcal{R} couplings $\lambda_{122} = 10^{-3}$: $M(h^0) \sim M(bb)$ - for reconstructed b jets originating from h^0 's. The ISR, FSR and hadronization are switched on. The arrows point to the theoretical values of m_{h^0} in each SUGRA point.

Muons are reconstructed if they are in the acceptance region (typically $|\eta| < 2.5$) and their energies and directions are obtained from the simulated one by a parametrized smearing function of ATLFAST. In most cases these functions were determined or cross checked by detailed simulation using GEANT. Finally, the missing transverse energy is calculated.

3.3 Detection and identification efficiencies

The output of ATLFAST is written in a column-wise ntuple (CWN) for further analysis using PAW [22]. This ntuple contains all the reconstructed electron, muon and jet objects together with the two transverse components of the missing energy. In addition, we have stored among the originally simulated particles and partons by RPV_ISAJET those which were produced in the decay chain of the generated SUSY particles. We have installed a bidirectional pointer between the reconstructed objects and the original particles/partons, and we have reinstated the mother-daughter relationships between the stored original particles/partons. A special record containing the integrated luminosity has been also included.

As a first step in the analysis we have randomly rejected reconstructed electrons and muons using a tabulated detection (including identification) efficiency. The efficiencies, as a function of the transverse momentum and η , have been extracted from a version of ATLFAST (2.0) which was released after the bulk of our event simulation has been carried out (see Fig.4).

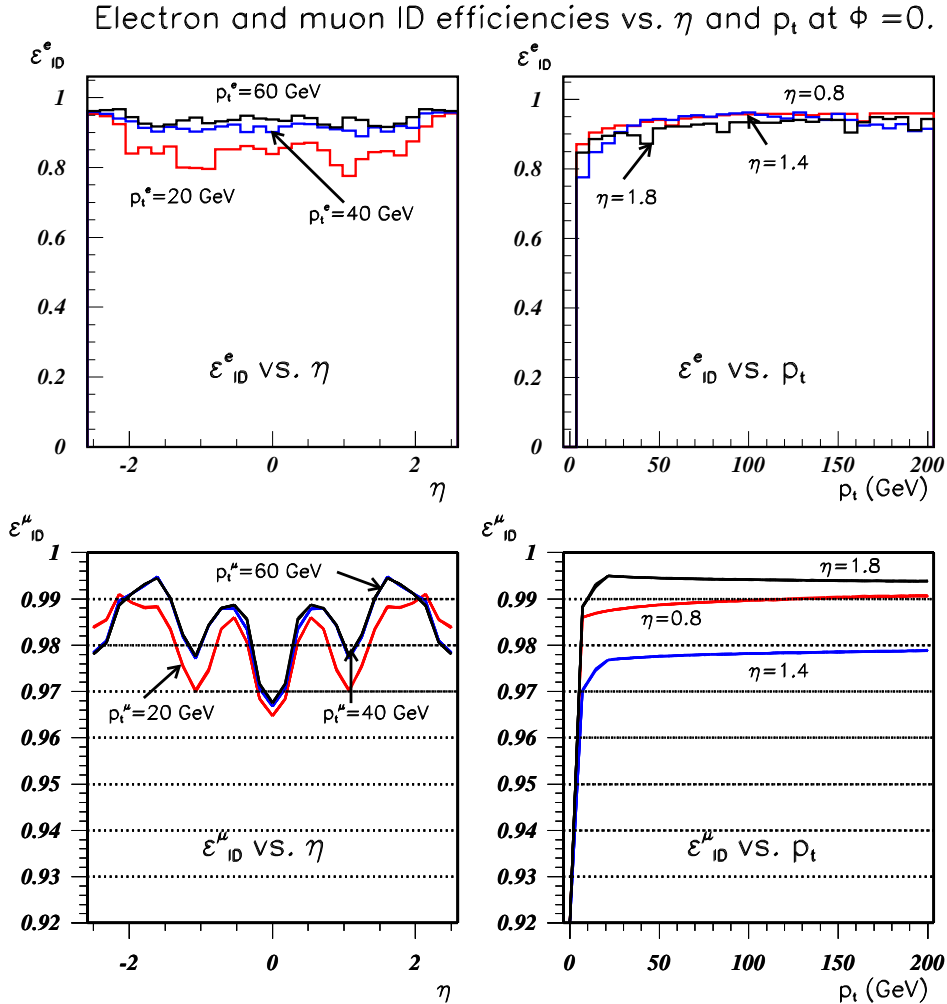


Figure 4: Detector efficiencies for muons and electrons as a function of p_t and η . The dependence on ϕ is practically negligible.

We have also randomly reclassified tagged b-jets to light jets with a b-tagging efficiency of 60% and vice versa using the mistagging probability of $\sim 2\%$. These numbers have been obtained in a separate study by detailed Monte Carlo simulation [23].

The obtained final state reconstructed particles were submitted to selection cuts in order to find an optimum signal of SUSY over the background. These criteria as well as the reconstruction algorithms are described in the forthcoming sections.

4 Inclusive measurements

By measuring global variables, like e.g. the number of leptons of a given flavour or the average p_t of a lepton in an event, or simply the number of events passing some selection criteria, we would like to answer the following three questions:

(i) what is the maximum domain in the SUGRA parameter space in which ATLAS is sensitive for R parity violation;

(ii) can we determine the approximate energy scale of a SUGRA signal;

(iii) can we determine the dominant type of the different couplings which causes the signal.

For all these studies as well as for the exclusive measurements we have fixed the values of the λ_{ijk} couplings to 10^{-3} . We remind the reader that the event topology does not depend on the particular value of λ if it is between 10^{-2} and 10^{-4} .

Sensitivity of ATLAS in the SUGRA space

We have generated 1000 events in each of the 16×16 equally spaced points in the $m_{1/2}$ vs m_0 plane the other parameters being fixed (see Table2). We have generated the SM background events as given in Table3. Since the signature of the SUGRA event is characterized by multileptons and missing energy, we have tried several event selection based on the variation of the number of electrons and muons, their transverse energy and the value of the missing energy. We have used the quantity called significance:

$$S = N_{sig} / \sqrt{N_{bg}} \quad (6)$$

to delimitate the sensitive region with $S \geq 5$, where N_{sig} is the number of the accepted SUGRA events and N_{bg} is the number of accepted SM events. The sensitive region extending to the highest value of m_0 and $m_{1/2}$ has been obtained using the selection criteria:

1. $N_l \geq 3$
2. $E_t^{miss} \geq 100$ GeV
3. $p_t^1 \geq 70$ GeV
4. $p_t^l \geq 20$ GeV

where N_l is the total number of e and μ , p_t^1 is the highest transverse momentum of the leptons, p_t^l is the transverse momentum of the other leptons in the event. The first two cuts reject almost all SM background coming from the decay of heavy SM particles. The Standard Model processes generally does not fulfill at the same time both constraints. Z pair production (by Drell-Yan or in the t, u channels) with $Z \rightarrow l^+ + l^-$ give a higher multiplicity of leptons but with a very low E_t^{miss} (one of the leptons falling out the detector acceptance could mime a E_t^{miss} but will decrease the lepton multiplicity). W^\pm pair production (by Drell-Yan or in the t, u channels) and the associated production of W 's with Z 's give a higher E_t^{miss} through the neutrinos but proportionally less leptons. The $t\bar{t}$ production with $W^\pm \rightarrow \nu_l + l^\pm$ and the leptons arising from b jets reconstructed as isolated gives a higher E_t^{miss} but is generally suppressed by the isolation criteria of leptons.

The associated production Zjj is similar to the above mentioned cases.

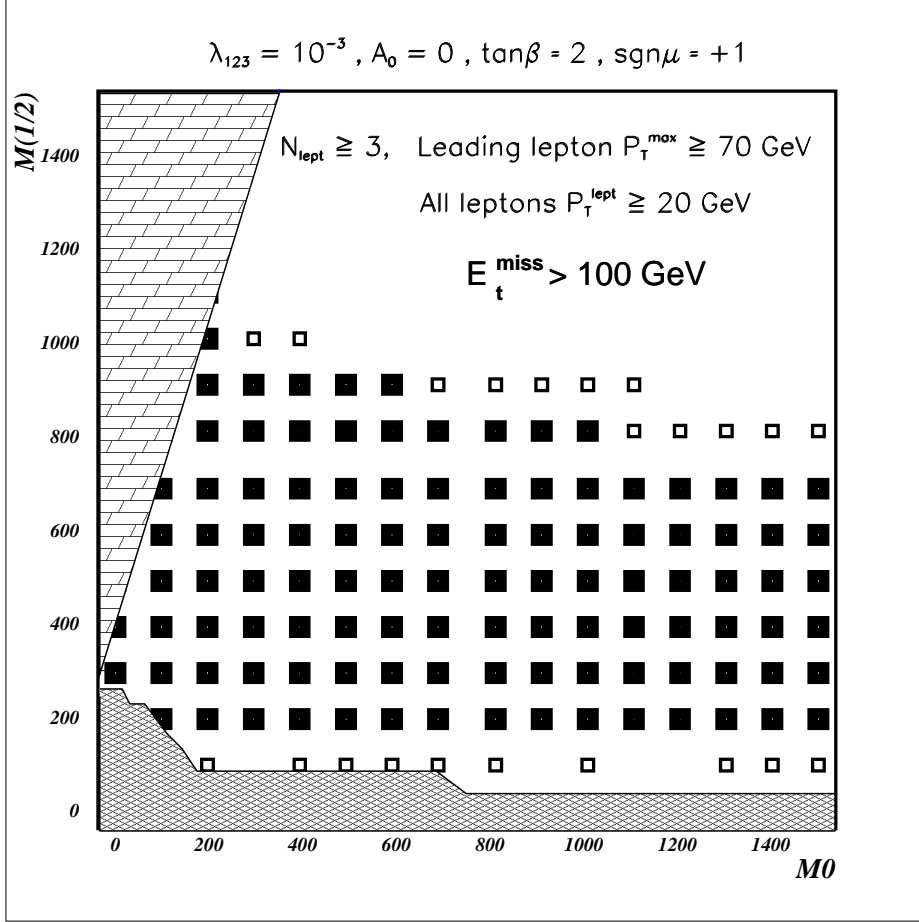


Figure 5: Sensitive domain in the SUGRA parameter space. For the explanation of the symbols see the text. The bricked domain is excluded by theory and the cross hatched one is excluded by experimental measurements.

Fig.5 shows the domain of the sensitivity one can obtain in 1 year of running with LHC at low luminosity. Due to the limited number of simulated events (which is much less than one can detect in one year) we have an uncertainty on this region: full squares indicate the grid points where $S > 5$ at 99% CL, no symbols at the grid points indicate that $S < 5$ at 99% CL, finally the open squares correspond to the cases where one cannot make any of the two above statements.

Energy scale of the SUGRA signal

If a SUSY signal manifests itself, its energy scale can be determined in the case when R parity is conserved from the distribution of the quantity [3]:

$$M_{eff} = \sum_{i=1}^4 p_{t,i}^j + E_t^{miss} \quad (7)$$

where $p_{t,i}^j$ are the 4 jets with the highest transverse momentum. The missing transverse energy, E_t^{miss} originates mainly from the $\tilde{\chi}_1^0$ decay. In the case of R parity violation we should therefore replace E_t^{miss} by the decay products of the $\tilde{\chi}_1^0$, i.e. we have used instead

of the definition (7) the following one:

$$M_{eff} = \sum_{i=1}^4 p_{t,i}^j + \sum_{i=1}^4 p_{t,i}^l + E_t^{miss} \quad (8)$$

where $p_{t,i}^l$ are the 4 leptons with the highest transverse momentum. The distributions of M_{eff} for the LHC point No 1 and 5 can be seen in Fig.6. The point No 1 (3rd line in Table 2) is associated with a high mass scale, whereas the point No 5 (5th line in Table 2) corresponds to a medium mass scale. This is well reflected in Fig.6.

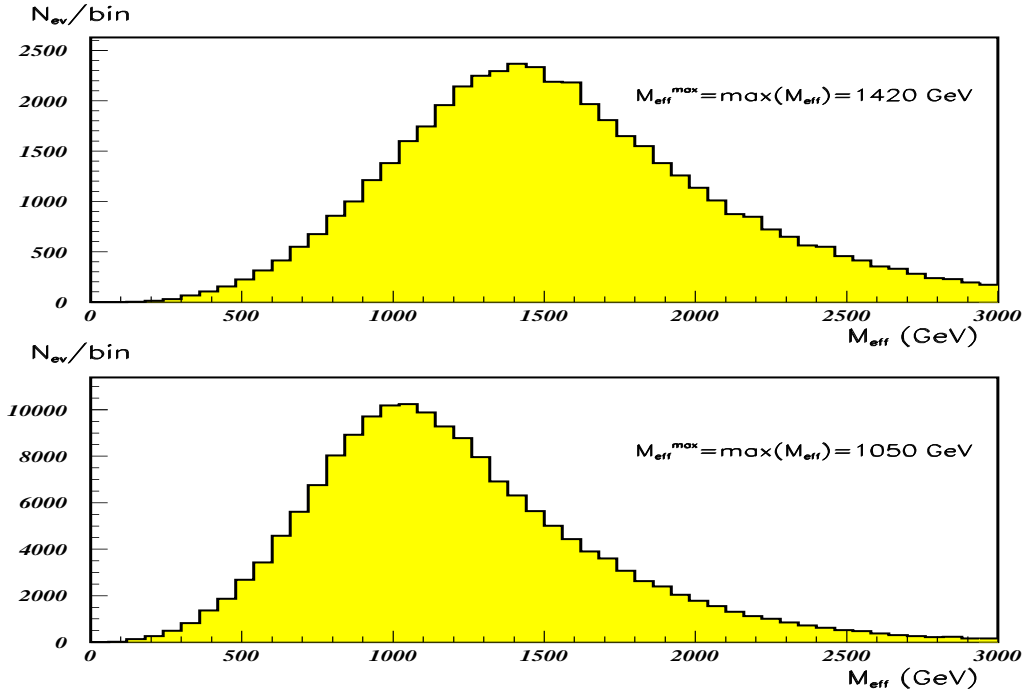


Figure 6: Distribution of M_{eff} for the LHC points No 1 and 5 after 3 years of LHC run at low luminosity. The inclusive cuts used here for both points are ($\lambda_{122} = 10^{-3}$): $N_{leptons} \geq 4$ and $E_t^{miss} \geq 50 GeV$. The maximum in these distributions (M_{eff}^{max}) depends strongly on the mass parameters of the models being a good observable for the mass scale.

In order to see how the M_{eff} distributions are correlated with the SUGRA mass scale, we have chosen randomly 30 points in the region of $0 \leq m_0 \leq 500$ GeV and $0 \leq m_{1/2} \leq 500$ GeV. At each points we have generated 10 000 events (see 2nd line in Table 2) and determined the maximum of the M_{eff} distributions: M_{eff}^{max} . The events were selected requiring more than 3 leptons and missing transverse energy higher than 50 GeV in an event. In the first plot of Fig.7 we show the correlation of this quantity with the SUGRA mass scale, M_{SUGRA} which we have defined as being the highest mass of the strongly interacting SUSY partners :

$$M_{SUGRA} = \min(m_{\tilde{g}}, m_{\tilde{q}_R}, m_{\tilde{b}_1}, m_{\tilde{t}_1}) \quad (9)$$

The observed strong correlation is even more pronounced in the second plot of Fig.7 where the distribution of the ratio of M_{eff}^{max}/M_{SUGRA} is shown.

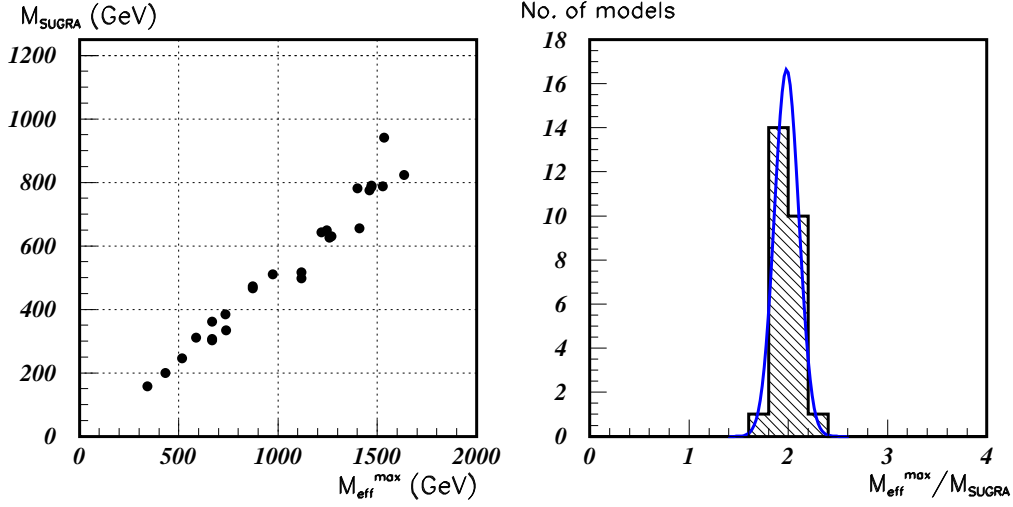


Figure 7: Correlation between M_{eff}^{max} and M_{SUGRA} and the distribution of the ratio M_{eff}^{max}/M_{SUGRA} for 30 SUGRA points (for other explanations see the text).

We have introduced another quantity to characterize the SUGRA energy scale in the case of R parity violation. Indeed, the algebraic sum of the lepton transverse momentum divided by the number of leptons:

$$p_t^{l, norm} = \left(\sum_{i=1}^4 p_{t,i}^l \right) / N^l \quad (10)$$

gives a correlation with m_0 and $m_{1/2}$ as shown in Fig.8, where the symbols delimitate the regions where $p_t^{l, norm}$ is higher than a certain value. On this plot we have selected events with $N_{lept} \geq 3$, $E_t^{miss} > 50$ GeV, and required a minimum value of 15 GeV for the momentum of any of the leptons and 50 GeV for the leading one.

Sensitivity for the type of the coupling

As mentioned in Section 2.1 counting the number of stable leptons not only can reveal the signal of R parity violation but also can give a hint on the type of the coupling which is realized. In order to show this we have simulated events in three different points of the SUGRA space (LHC No 1,3 and 5, see lines 3-5 of Table 2) and for two different couplings: λ_{122} and λ_{123} . In the Table 4 the number of events are given one can observe for the two classes: $0e + 4\mu$ and $4e + 0\mu$ in one year of LHC running at low luminosity. The events satisfy the following criteria:

$$\begin{aligned} 20 \leq p_t^l \leq 250 \text{ GeV and } E_t^{miss} \geq 250 \text{ GeV at points 1 and 5} \\ 10 \leq p_t^l \leq 100 \text{ GeV and } E_t^{miss} \geq 150 \text{ GeV at point 3.} \end{aligned}$$

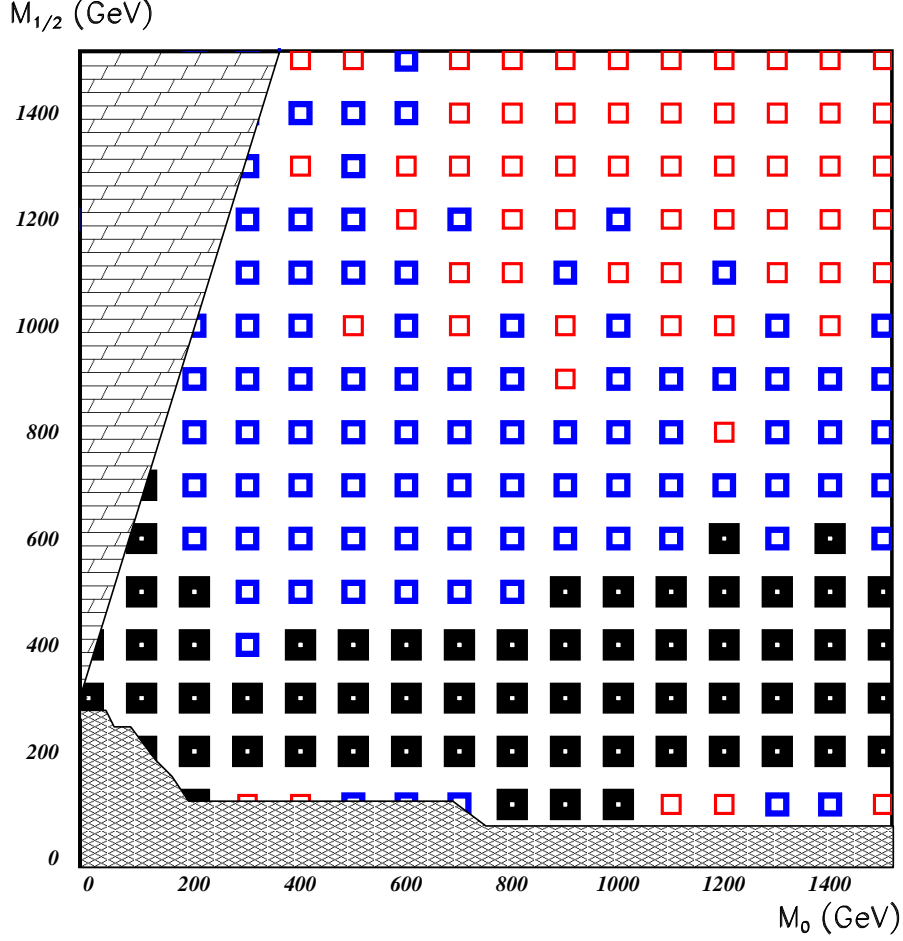


Figure 8: In the case of $\lambda_{123} = 10^{-3}$, $A_0 = 0$, $\tan\beta = 2$, $\text{sign}\mu = +1$ and for the global cuts : $N_{lept} \geq 3$, $E_t^{miss} \geq 50$ GeV, $p_t^l \geq 15$ GeV and $p_t^{l,max} \geq 50$ GeV one can "divide" the $(m_0, m_{1/2})$ space in $p_t^{l, norm}$ domains: - full squares: $p_t^{l, norm} \in (30, 150)$ GeV; - fat squares: $p_t^{l, norm} \in (150, 250)$ GeV; - open squares: $p_t^{l, norm} \in (250, 500)$ GeV. Bricked domain is excluded by theory and the hatched one is excluded by the present experimental limits.

Table 4: Number of events with different number of electrons and muons

	λ_{122}		λ_{123}	
	$0e + 4\mu$	$4e + 0\mu$	$0e + 4\mu$	$4e + 0\mu$
Point No 1	934 ± 16	3 ± 1	76 ± 4	68 ± 4
Point No 5	3010 ± 52	20 ± 4	289 ± 17	304 ± 18
Point No 3	52636 ± 1760	3356 ± 444	12400 ± 600	15565 ± 672

It is obvious that one can clearly distinguish which of the two couplings are realized in Nature. This is further illustrated in Fig.9, where we have plotted the distribution of the number of muons/event for the two different couplings where the total number of electrons and muons is equal to four.

To conclude this section we have demonstrated that even if R parity is violated ATLAS can detect the signal of SUGRA in a large domain of the parameter space. This domain is compatible with that obtained in the case when R parity is conserved. We can equally well establish the mass scale of the SUGRA compared to the case of R parity conservation. Finally, one has a possibility to determine the type of the coupling if only one causes the violation of the R parity.

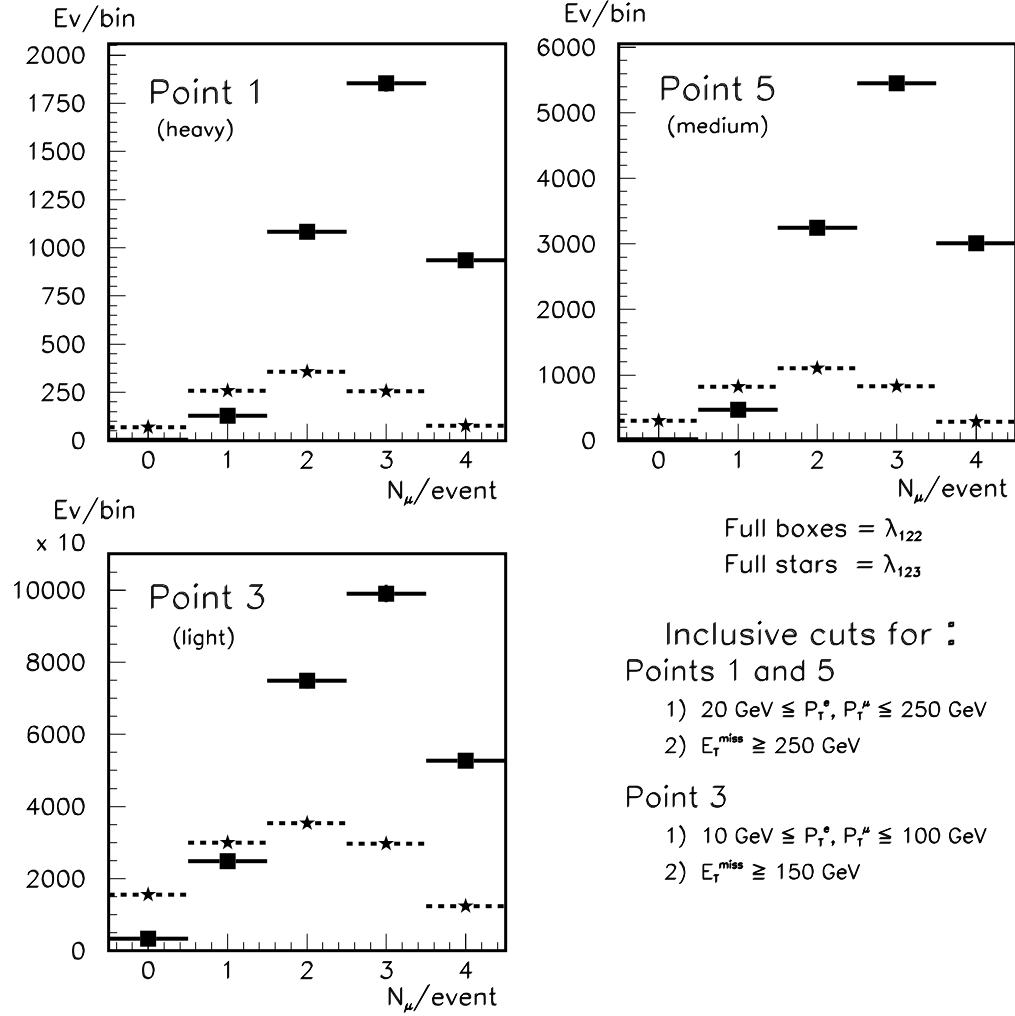


Figure 9: The distribution of the number of muons per event if the total number of electrons and muons is equal to 4 in the case of two R couplings (λ_{122} , λ_{123}) in the SUGRA points 1, 3 and 5.

5 Exclusive measurements

In this chapter we show that one can determine the parameter values of the SUGRA model, similarly to the case when R parity is conserved [4]-[7]. The quantities to be used for this purpose, in general, are the masses of the reconstructed SUSY particles as well as their observed production cross sections and branching ratios. We shall use only the first type of characteristics in this analysis since determination of cross sections and branching ratios is more sensitive to the acceptances and in many cases detailed simulations are needed. In 3 out of the 5 LHC points, which are sufficiently different to illustrate the methods in various conditions, we shall first show how to reconstruct the SUSY particles, determine their masses, and finally fit the model parameters to these mass values.

The reconstruction of the SUSY particles are difficult because there are always at least two final state particles which cannot be detected. These are obviously the LSP's in the case of R parity conservation, but if R parity is violated through the terms (3) there is always at least one undetectable neutrino produced in each LSP decay (see also Table 1). To overcome this difficulty we use the fact that in a 3-body decay:

$$A \longrightarrow a b c \quad (11)$$

the invariant mass m_{bc} of two of the three final state particles, e.g. b and c gives a clear endpoint. The endpoint, m_{bc}^{end} is related to the masses of A and that of the undetected particle, a :

$$m_{bc}^{end} = m_A - m_a \quad (12)$$

since in the restframe of A the three-momentum of a (or that of the (bc) system) is zero. This equation is particularly useful if the mass of a is zero: in this case one can directly estimate the mass of the particle A by measuring the endpoint of the m_{bc} distribution. Of course, in the practice this measurement is difficult because the endpoint may be hidden by eventual background and it can disappear if either b or c is unstable. This is the case when a τ is produced in the decay of the $\tilde{\chi}_1^0$, thus in all couplings when a "3" appears in the index of the λ .

Once the endpoint is established one can determine even the four-momentum P^μ of the undetected particle a or that of the mother particle A by selecting events around the endpoint:

$$P_{A,a}^\mu = \frac{m_{A,a}}{m_{bc}} (P_b^\mu + P_c^\mu) \quad (\mu = 1, \dots, 4) \quad (13)$$

As one can see from Eqs. (12) and (13), if particle a has zero mass (as e.g. in the case of a neutrino), the four-momentum of the charged lepton pair is equal to that of particle A . The four-momentum of particle A can be used further for the reconstruction of the parent particle, and so on, until one arrives at the beginning of the decay chain, i.e. at the original SUSY particle. It is also obvious that at the endpoint the 4-momentum of particle a and A are parallel whatever their masses are.

Since equations (12) and (13) are strictly valid only at the endpoint, one usually needs a large number of produced events and in the selection of the size of the region around the endpoint an optimum has to be found between the statistical error and the approximate validity of the above relations. In practice one applies in Eq.(13) m_{bc} instead of m_{bc}^{end} in order to "rescale" the values of $P_b^\mu + P_c^\mu$ which are smaller than their corresponding values at the endpoint.

5.1 The LHC points No1 and No5

Concerning the reconstruction of the SUSY particles these two points are very similar and therefore we treat them here together. In the cascade decay chain (*) the predominant decay of the $\tilde{\chi}_2^0$ proceeds via $\tilde{\chi}_2^0 \longrightarrow h^0 + \tilde{\chi}_1^0$ with a BR of $\sim 99\%$ in point 1 and $\sim 63\%$ in point 5, where the competitive decay through \tilde{l}_R becomes also important.

The main inclusive cuts to select SUSY events are based on the requirement of a high lepton multiplicity, $N_l \geq 4$ and a moderate missing transverse energy, E_t^{miss} .

The SM background is small and can be completely neglected applying a cut on E_t^{miss} as is shown in Fig.10 where the E_t^{miss} distribution is shown for the points 1 and 5 and for λ_{122} and λ_{123} .

Table 5: SUSY particle masses at points 1, 3 and 5 in GeV

LHC point	1	3	5
\tilde{g}	1008	299	769
\tilde{q}_L	958	317	687
\tilde{q}_R	925	312	664
\tilde{b}_2	922	313	662
\tilde{b}_1	855	278	634
\tilde{t}_2	913	325	706
\tilde{t}_1	649	260	494
\tilde{l}_L	490	216	239
\tilde{l}_R	430	207	157
$\tilde{\nu}_L$	486	207	230
$\tilde{\tau}_2$	490	216	239
$\tilde{\tau}_1$	430	206	157
$\tilde{\chi}_2^\pm$	775	274	526
$\tilde{\chi}_1^\pm$	326	96	232
$\tilde{\chi}_4^0$	778	275	529
$\tilde{\chi}_3^0$	762	258	505
$\tilde{\chi}_2^0$	326	97	233
$\tilde{\chi}_1^0 = \text{LSP}$	168	45	122
h_0	98	69	95

The "structures" seen in the hatched histograms of Fig.10 is due to statistical fluctuations. In what follows we shall demonstrate that in the case of the coupling λ_{122} we can reconstruct all the SUSY particles in the decay chain (*), starting with the $\tilde{\chi}_1^0$, and in this respect we can achieve more than it was the case with R parity conserved. On the other hand, if λ_{123} is nonzero, we can reconstruct only a fraction of the SUSY particles, and the decay products of the $\tilde{\chi}_1^0$, i.e. the additional leptons, increase the background and thereby deteriorate the determination of some particle masses. We shall show that in spite of these difficulties the achieved precision is at worst comparable with the one in the case of conserved R parity.

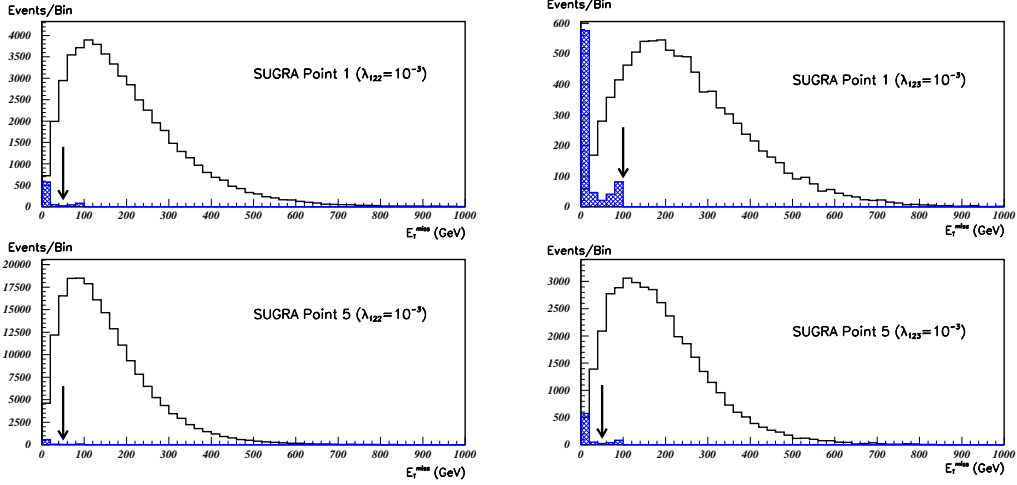


Figure 10: The distribution of E_t^{miss} for SUSY events (open histogram) and SM events (hatched histogram) in points 1 and 5 for $\lambda_{122} = 10^{-3}$ (left plots) and $\lambda_{123} = 10^{-3}$ (right plots) for events with $N_{leptons} \geq 4$, $P_t^{lept} \geq 10$ GeV and after 3 years of LHC run at low luminosity. The arrows precise the cuts to be used.

The case $\lambda_{122} \neq 0$

Reconstruction of $\tilde{\chi}_1^0 \rightarrow \nu_{e(\mu)} + e^\pm(\mu^\pm) + \mu^\mp$

For the reconstruction of the $\tilde{\chi}_1^0$ we apply the following selection criteria:

- (i) $N_l \geq 4$ (and $N_l^+ = N_l^-$ and $N_e = N_\mu$ for point 5),
- (ii) $p_t^l \geq 10$ GeV, $\cos(\alpha_{l^\pm l'^\mp}) \geq 0.5$,
- (iii) $E_t^{miss} \geq 50$ GeV ,

where $\alpha_{l^\pm l'^\mp}$ is the angle between any OSDF (i.e. electron -muon) leptons.

The invariant mass distributions of the OSDF lepton pairs are shown in Fig.11 for point 1 and in Fig.12 for point 5, where the number of events correspond to 3 years of LHC run at low luminosity.

In point 1, isolated leptons are produced practically only in the two \tilde{R} decays of the $\tilde{\chi}_1^0$'s, therefore the background of OSDF distribution will be mainly $\tilde{\chi}_1^0$ combinatorial. In point 5, as we mentioned before, a non-negligible production of isolated leptons (beyond the \tilde{R} decays of $\tilde{\chi}_1^0$'s) comes from $\tilde{\chi}_2^0 \rightarrow \tilde{l}_R^\pm + l^\mp \rightarrow \tilde{\chi}_1^0 + l^\pm + l^\mp$. This decay will produce two leptons of opposite sign (OS) but of the same flavor (SF), changing the balance of leptons per flavor. Most of the events with an increased number of leptons, will have only one $\tilde{\chi}_2^0$ decaying leptonically (the other one, if it exists, will decay in h^0 's). To decrease the number of bad combinations (with leptons not coming from $\tilde{\chi}_1^0$'s), additional cuts like $N_l^+ = N_l^-$ and $N_e = N_\mu$ in each event are very efficient.

There is a clear endpoint over a moderate background at both points 1 and 5 corresponding to the $\tilde{\chi}_1^0$ mass (c.f. Table5) in virtue of Equ.(12). We parametrize and subtract the background with a Maxwellian distribution and fit the resulting distribution near the endpoint obtaining the $\tilde{\chi}_1^0$ mass values:

$$m_{\tilde{\chi}_1^0}^{mas} = 169.80 \pm 0.07 \text{ GeV at point 1} \quad (16)$$

$$m_{\tilde{\chi}_1^0}^{mas} = 122.62 \pm 0.35 \text{ GeV at point 5} \quad (17)$$

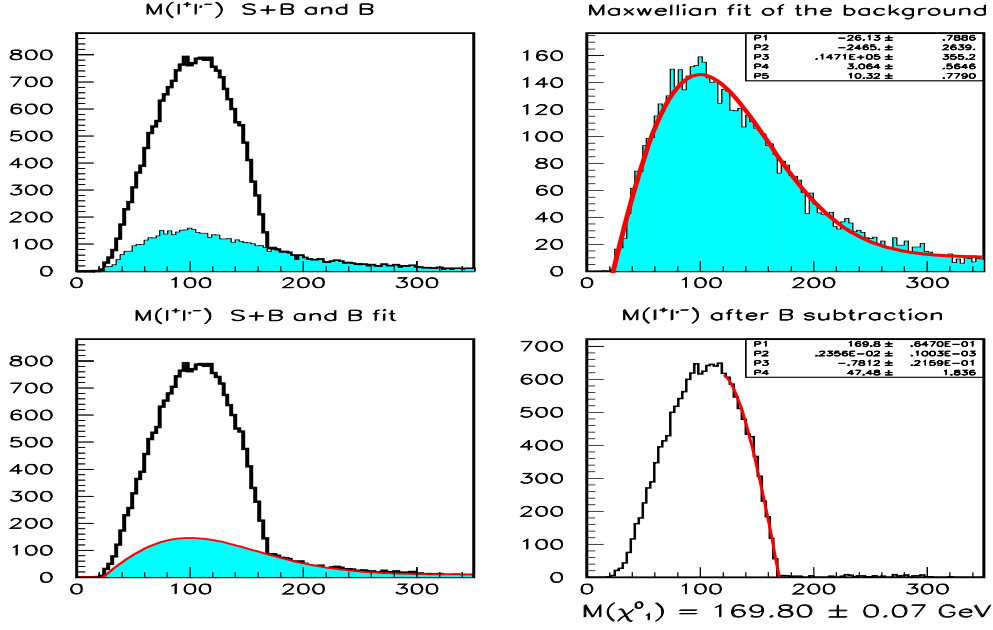


Figure 11: The invariant mass distribution of the OSDF lepton pairs for 3 years of LHC run at low luminosity at point 1 (for the selection criteria see text). In the upper-left plot are represented all events (open histogram) and the background (shaded histogram) which is mainly SUSY combinatorial. The upper-right and lower-left plots show a Maxwellian-like distribution fitted to the background. The lower-right plot represents the result after the subtraction of the fitted background. The edge is fitted with a polynomial function and the error is only statistical.

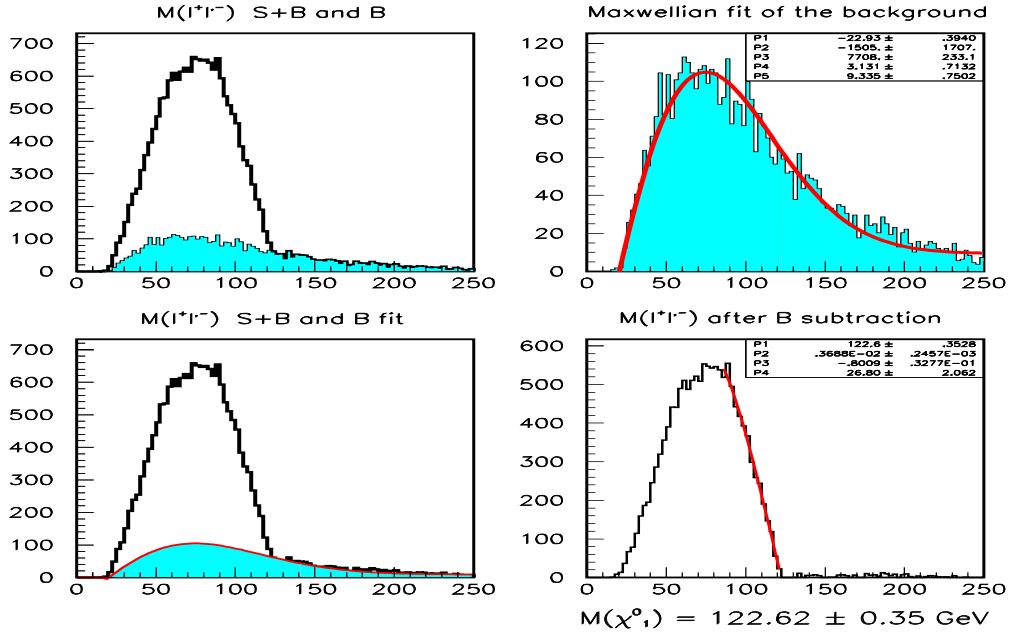


Figure 12: The invariant mass distribution of the OSDF lepton pairs for 3 years of LHC run at low luminosity at point 5 (for the selection criteria see text).

The estimated error contains both statistical and systematical. This latter is due to the energy resolution of the leptons and mainly to the finite bin-size of our histograms around the endpoint. Since due to the bin-size one tends to overestimate the mass value the systematical error is asymmetrical.

For any further reconstruction using OSDF pairs (like $\tilde{\chi}_2^0$, $\tilde{\chi}_1^\pm$, etc) one will take as $\tilde{\chi}_1^0$ candidates the OSDF pairs with an invariant mass in $(m_{\tilde{\chi}_1^0} - \Delta m_{\tilde{\chi}_1^0}, m_{\tilde{\chi}_1^0})$, where $\Delta m_{\tilde{\chi}_1^0} = 50$ GeV for point 1 and $\Delta m_{\tilde{\chi}_1^0} = 30$ GeV for point 5. To improve the statistics in point 5 we will not use the additional cuts (see (i)).

Reconstruction of $h^0 \rightarrow b + \bar{b}$

To the global cuts ($N_l \geq 4$, $P_t^l \geq 10$ GeV and $E_t^{miss} \geq 50$ GeV) we will add some specific cuts on b jets. Since the h^0 decays to $b\bar{b}$ pairs with appr. 88% BR its reconstruction proceeds by the selection of these pairs, adding thus the following detection criteria to the above ones:

(iv) $p_t^b \geq 30$ GeV for point 1, 40 GeV for point 5 respectively, and $p_t^b \leq 300$ GeV for both points

(v) $\cos(\alpha_{b\bar{b}}) \geq 0.4$ (point 1) or 0.3 (point 5)

where $\alpha_{b\bar{b}}$ is the angle between the b and \bar{b} . The obtained invariant mass distributions of the $b\bar{b}$ pairs are shown in Fig.14 and Fig.15. There is a clear mass peak corresponding to the h^0 particle (c.f. Table5).

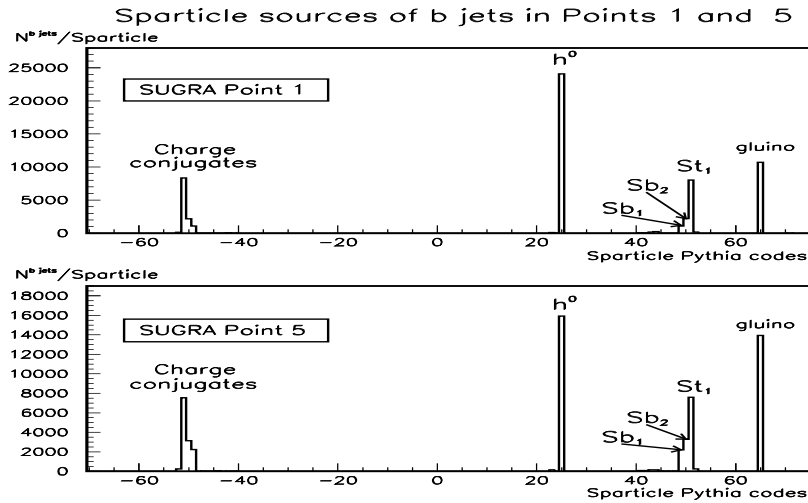


Figure 13: The sparticle mothers of b jets (in Pythia codes) in the points 1 and 5 (see text).

As we can see from the Fig.13, the b jets are mainly produced through $h^0 \rightarrow b\bar{b}$ but also through $\tilde{g} \rightarrow \tilde{b}_{1(2)} + \bar{b} \rightarrow \tilde{\chi}_{1(2)}^0 + b + \bar{b}$ or $\tilde{g} \rightarrow \tilde{t}_1 + \bar{t} \rightarrow \tilde{\chi}_{1(2)}^0 + t + \bar{t}$ (or $\rightarrow \tilde{\chi}_1^+ + b + \bar{t}$) and the subsequent decay of t . In the case of conserved R this SUSY background (as well as the SM $t\bar{t}$) is efficiently rejected with a veto on leptons (coming from the top decay). However, in the case of R through L couplings we cannot apply anymore such a cut (and a veto on *additional* leptons doesn't increase significantly the S/B ratio). Another source of background (albeit small) is the production of Z 's (i.e. $\tilde{t}_2 \rightarrow \tilde{t}_1 + Z^0$ or $\tilde{\chi}_i^0 \rightarrow \tilde{\chi}_1^0 + Z^0$, $i = 2, 3, 4$ or $\tilde{\chi}_2^\pm \rightarrow \tilde{\chi}_1^\pm + Z^0$, with $Z^0 \rightarrow b + \bar{b}$) resulting in a peak very close to the h^0 one. This will give rise to an asymmetric h^0 peak with a higher width as can be seen in both points. A similar effect arises also from the calibration error of b jets.

After having parametrized and subtracted this background we have fitted the mass peak with a Gaussian curve and obtained the values:

$$m_{h^0}^{meas} = 97.08 \pm 0.62 \text{ GeV at point 1} \quad (18)$$

$$m_{h^0}^{meas} = 94.7 \pm 0.64 \text{ GeV at point 5} \quad (19)$$

The estimated systematic error is mainly due to the uncertainties in the b -jet correction factor shown in Fig.2.

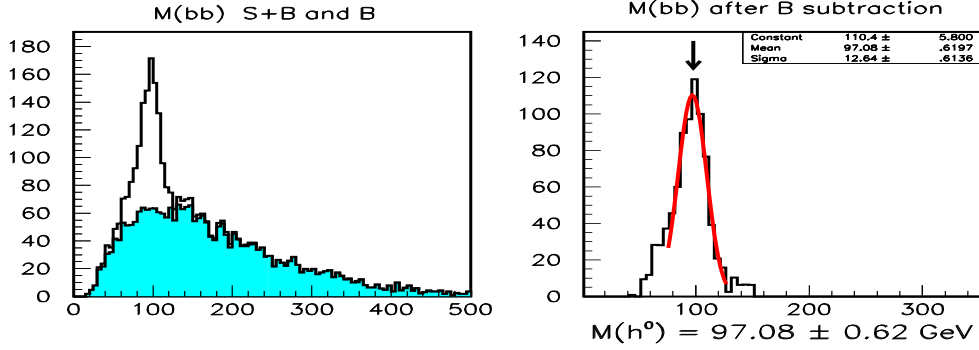


Figure 14: The invariant mass distribution of the $b\bar{b}$ pairs for 3 years of LHC run at low luminosity at point 1. On the left plot are represented all the events and the background (shadowed). The background is fitted with a Maxwellian function and subtracted. The result is drawn in the right plot. The arrow points to the theoretical value of m_{h^0} . The peak is fitted with a gaussian. The written error contains only the statistical part.

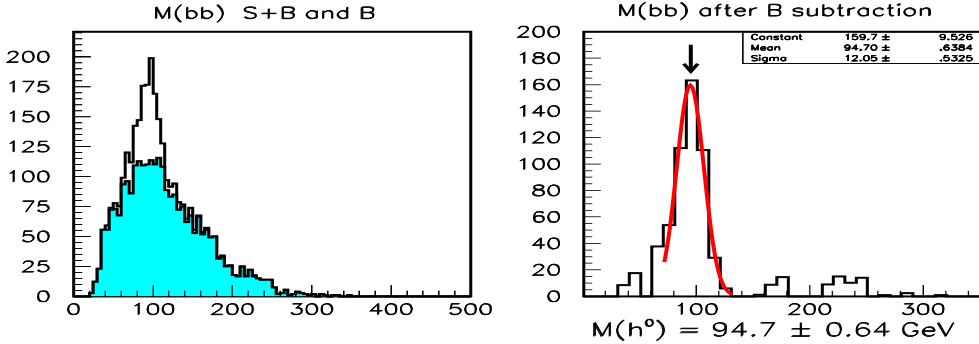


Figure 15: The invariant mass distribution of the $b\bar{b}$ pairs for 3 years of LHC run at low luminosity at point 5.

Reconstruction of $\tilde{\chi}_2^0 \rightarrow h^0 + \tilde{\chi}_1^0$

The reconstructed h^0 and $\tilde{\chi}_1^0$ allows the reconstruction of the mother particle, the $\tilde{\chi}_2^0$, since this latter decays to the formers by 99% BR at point 1 and 63% BR at point 5. We will require the $\tilde{\chi}_1^0$ candidates (OSDF lepton pairs) to be "close" to the endpoint :

$$(vi) m(OSDF) \in (m^{endp} - 50, m^{endp}) \text{ GeV - in point 1 and,}$$

$m(OSDF) \in (m^{endp} - 30, m^{endp})$ GeV - in point 5,
and the h^0 candidates (bb pairs) to be around the mass peak of h^0 :

(vii) $m(bb) \in (m^{peak} - 15, m^{peak} + 15)$ GeV - for both points 1 and 5.

Looking at the relations between $\tilde{\chi}_2^0$, $\tilde{\chi}_1^0$ and h^0 masses, one can expect in point 1 a higher boost of $\tilde{\chi}_1^0 - h^0$ pair, comparing to point 5, therefore we demand :

(viii) $\cos(\alpha_{h_0\tilde{\chi}_1^0}) \geq 0.7$ (point 1) or 0.5 (point 5).

Finally one gets the invariant mass distributions of the $h_0\tilde{\chi}_1^0$ pairs as shown in the Fig.16. The background in this case is combinatorial on the one hand, and comes from SUSY production of $t\bar{t}$ pairs with : $t\bar{t} \rightarrow b + W^+ + \bar{b} + W^- \rightarrow b + \bar{b} + l^+ + l^- + \nu_l + \bar{\nu}_l$ on the other hand. However, the strong correlation required separately between the leptons and between the b jets will suppress it considerably.

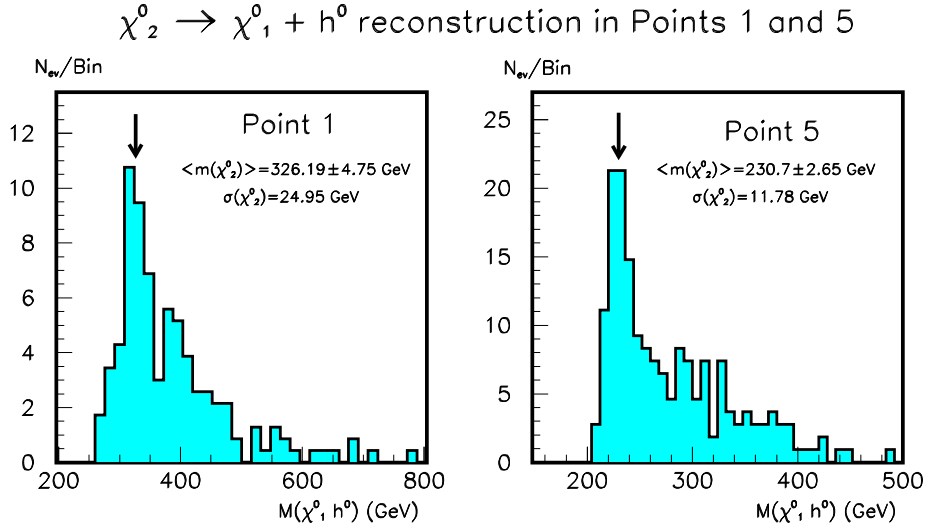


Figure 16: The invariant mass distribution of the $h_0\tilde{\chi}_1^0$ pairs for 3 years of LHC run at low luminosity in points 1 and 5. The tail is due to bad combinations with the wrong $\tilde{\chi}_1^0$. The arrows point to the theoretical values of $m_{\tilde{\chi}_2^0}$. The masses are determined by a gaussian fit around the peak. The error is only the statistical.

The peak around the $\tilde{\chi}_2^0$ mass value (c.f. Table 5) allows to estimate this latter by fitting a Gaussian curve on the peak:

$$m_{\tilde{\chi}_2^0}^{meas} = 326.19 \pm 4.75 \text{ GeV at point 1} \quad (20)$$

$$m_{\tilde{\chi}_2^0}^{meas} = 230.7 \pm 2.65 \text{ GeV at point 5} \quad (21)$$

Reconstruction of $\tilde{\chi}_1^\pm \rightarrow \tilde{\chi}_1^0 + W^\pm$

The same technique allows the reconstruction of the lightest chargino ($\tilde{\chi}_1^\pm$). As one can see in the scheme (*) one reconstructs first the W^\pm . The W reconstruction is carried out by combining light quark jet pairs using the additional selection criteria (to (i ÷ iii) and (vi)):

(ix) $p_t^j \geq 100$ GeV and $p_t^j \leq 600$ GeV (point 1) or 350 GeV (point 5)

(x) $\cos(\alpha_{jj}) \geq 0.9$ (point 1) or 0.87 (point 5)

where α_{jj} is the angle between the jj pair. The obtained invariant mass distributions of the jj pairs are shown in Fig.17. There is a clear mass peak at the place of the W mass. Selecting the W candidates around the W mass peak (± 15 GeV) and using the $\tilde{\chi}_1^0$ candidates close to the endpoint (see (vi)) we plot the invariant mass distribution of the $\tilde{\chi}_1^0 W$ pairs in Fig.17, by requiring that the $\tilde{\chi}_1^0$ and the W be close in phase space:

(xi) $\cos(\alpha_{W\tilde{\chi}_1^0}) \geq 0.85$ in both points

where $\alpha_{W\tilde{\chi}_1^0}$ is the angle between the $\tilde{\chi}_1^0 W$ pair.

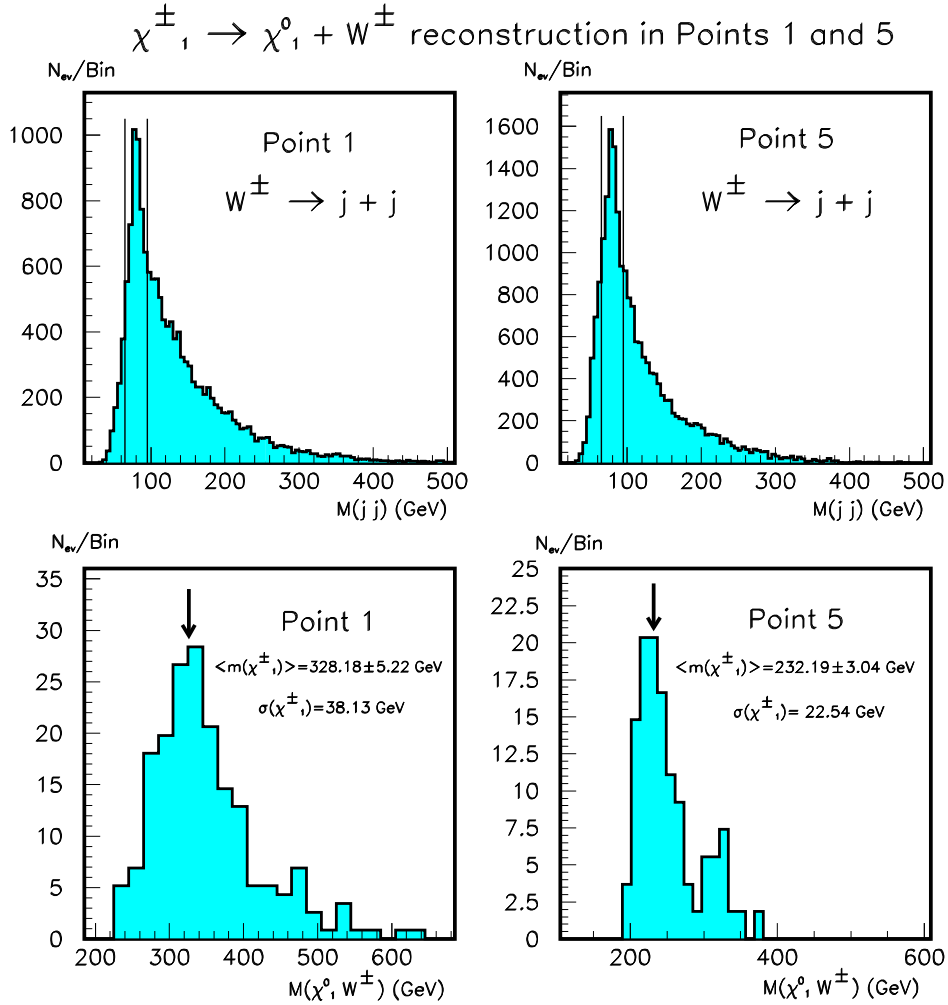


Figure 17: The invariant mass distribution of the jj pairs for 3 years of LHC run at low luminosity at point 1 and 5 (upper plots). Selecting W candidates around W mass peak (± 15 GeV - between the bars), we combine them with the $\tilde{\chi}_1^0$ candidates and obtain the distributions represented in the lower plots for point 1 and 5 respectively. The arrows point to the theoretical values for $m_{\tilde{\chi}_1^\pm}$.

One can see a clear peak at the mass value of the lightest chargino at point 5 (c.f. Table5). At point 1, where the statistics is much more limited due to the heaviness of

The obtained invariant mass distributions of the $j\tilde{\chi}_1^0$ pairs are shown in Fig.18. The \tilde{q}_R can be produced directly in the hard process or in the decay of \tilde{g} . In points 1 and 5 the jet associated with \tilde{q}_R is very soft comparing to the jet associated with $\tilde{\chi}_1^0$ and often the soft jet can fall in the cone of the reconstructed hard jet. This is the reason of the presence of a shoulder at the \tilde{g} mass value in the distributions of Fig.18. Another source of background is the decay $\tilde{q}_L \rightarrow \tilde{\chi}_1^\pm + q$ with $\tilde{\chi}_1^\pm \rightarrow \tilde{\chi}_1^0 + W^\pm \rightarrow \tilde{\chi}_1^0 + \nu_l + l^\pm$ and l^\pm undetected. The left shoulder at the \tilde{t}_1 mass at point 5 corresponds to the case where the 3 jets of the $\tilde{t}_1 \rightarrow \tilde{\chi}_1^+ + b \rightarrow \tilde{\chi}_1^0 + j + j' + b$ or $\tilde{t}_1 \rightarrow \tilde{\chi}_1^0 + t \rightarrow \tilde{\chi}_1^0 + j + j' + b$ decay chains are erroneously combined into a single energetic one. One can see mass peaks at the values of the right handed squarks (c.f. Table5). The obtained mass values will have large errors due to the superposition of all these effects :

$$m_{\tilde{q}_R}^{meas} = 931.7 \pm 11.37 \text{ GeV at point 1} \quad (24)$$

$$m_{\tilde{q}_R}^{meas} = 662.4 \pm 5.1 \text{ GeV at point 5} \quad (25)$$

Reconstruction of $\tilde{q}_L \rightarrow \tilde{\chi}_2^0 + \text{jet in point 5}$

For the point 5 we can do more due to the higher statistics. As we already mentioned in the case of \tilde{q}_R , the \tilde{q}_L can decay with a branching fraction of about 31 % in $\tilde{\chi}_2^0$ and a light jet. This jet is also very energetic. In addition to the cuts ($i \div viii$) one will select $\tilde{\chi}_2^0$ candidates from the $\tilde{\chi}_1^0 h^0$ distribution :

$$(xiv) m(\tilde{\chi}_1^0 h^0) \in (m_{\tilde{\chi}_2^0} - 40, m_{\tilde{\chi}_2^0} + 40) \text{ GeV}$$

and only one hard light-flavoured jet with :

$$(xv) p_i^{jet} \geq 100 \text{ GeV whose invariant mass with any other light jet is } \pm 15 \text{ GeV outside of the } W^\pm \text{ or } Z^0 \text{ masses.}$$

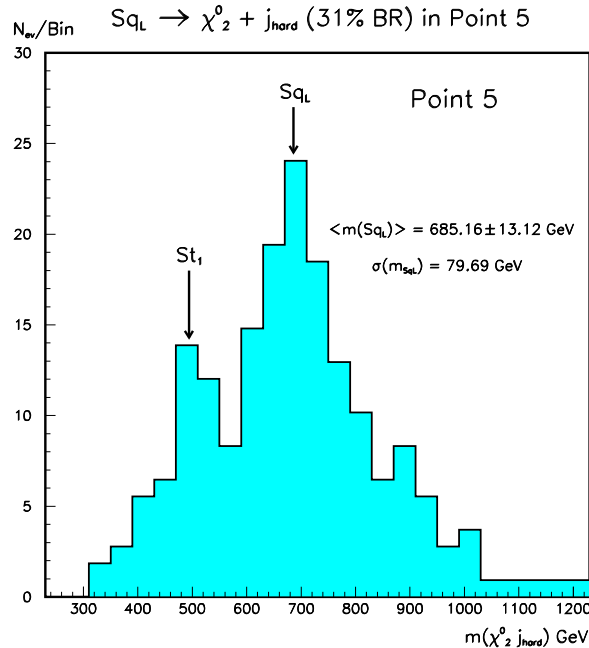


Figure 19: The invariant mass distribution of the $j\tilde{\chi}_2^0$ pairs for 3 years of LHC run at low luminosity at point 5. Vertical arrows point to the nominal values of \tilde{q}_L and \tilde{t}_1 masses. For cuts see text.

The decay $\tilde{t}_1 \rightarrow \tilde{\chi}_2^0 + t \rightarrow \tilde{\chi}_2^0 + j + j + b$ when the 3 jets are erroneously combined into a single hard jet, manifests itself as a peak at the \tilde{t}_1 mass (see Fig.19). The gaussian fits to these peaks, after three years of LHC run at low luminosity, result in :

$$m_{\tilde{q}_L}^{meas} = 685.16 \pm 13.12 \text{ GeV at point 5} \quad (26)$$

$$m_{\tilde{t}_1}^{meas} = 503.6 \pm 14.25 \text{ GeV at point 5.} \quad (27)$$

Reconstruction of $\tilde{l}_R^\pm \rightarrow \tilde{\chi}_1^0 + l^\pm$ in point 5

In the point 5, the \tilde{l}_R^\pm decays ~ 100 % in $\tilde{\chi}_1^0$ and l^\pm . In order to obtain the mass of the right handed slepton, we have combined the $\tilde{\chi}_1^0$ candidates with a "soft" lepton not participating in the $\tilde{\chi}_1^0$ reconstruction and satisfying:

$$(xvi) \quad 10 \leq p_t^l \leq 200 \text{ GeV}$$

$$(xvii) \quad \cos(\alpha_{l\tilde{\chi}_1^0}) \geq 0.5$$

where $\alpha_{l\tilde{\chi}_1^0}$ is the angle between the $l\tilde{\chi}_1^0$ pair. The obtained invariant mass distribution is shown in Fig.20. Besides the combinatorial one, the background arises from the decay $\tilde{\chi}_1^\pm \rightarrow \tilde{\chi}_1^0 + W^\pm \rightarrow \tilde{\chi}_1^0 + l^\pm + \nu_l$, which results in an *endpoint* in the $l^\pm\tilde{\chi}_1^0$ distribution at the mass of $\tilde{\chi}_1^\pm$.

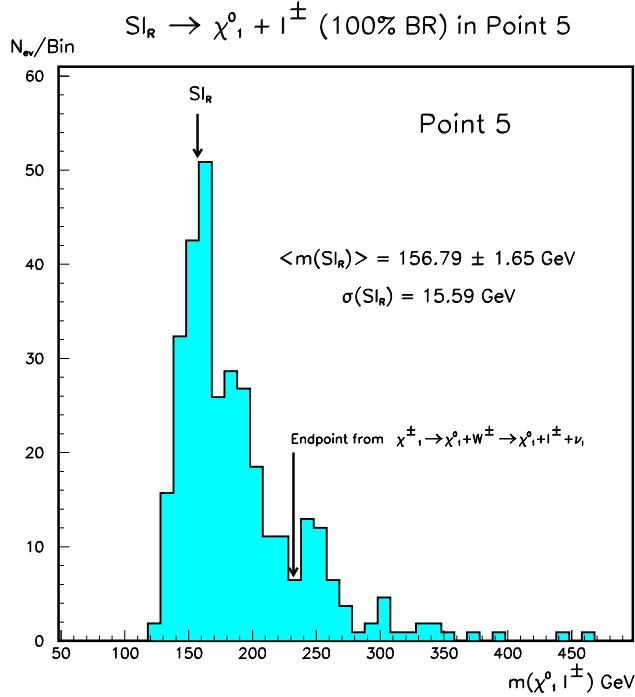


Figure 20: The invariant mass distribution of the $l\tilde{\chi}_1^0$ pairs for 3 years of LHC run at low luminosity at point 5. The arrows point to the nominal values of $m_{\tilde{l}_R}$ and $m_{\tilde{\chi}_1^\pm}$.

A gaussian fit to the mass peak gives :

$$m_{\tilde{l}_R}^{meas} = 156.8 \pm 1.65 \text{ GeV at point 5} \quad (28)$$

which agrees with the value of the right handed slepton (c.f. Table5).

The case $\lambda_{123} \neq 0$

As stated earlier, in this case there is always a τ particle among the decay products of the $\tilde{\chi}_1^0$, and this spoils the endpoint in the OSDF lepton pair mass distribution which would permit us to reconstruct $\tilde{\chi}_1^0$ and all the other sparticles further (see Fig.21 and compare with the upper left plot of Fig.12). Therefore, the strategy in the case of \tilde{R} couplings implying the third family of leptons must be changed, and consequently we shall *abandon the direct reconstruction of $\tilde{\chi}_1^0$, and return to the strategy developed in the case of conserved R parity.* In other words, we shall discard the decay products of $\tilde{\chi}_1^0$ in the first stage of the reconstruction.

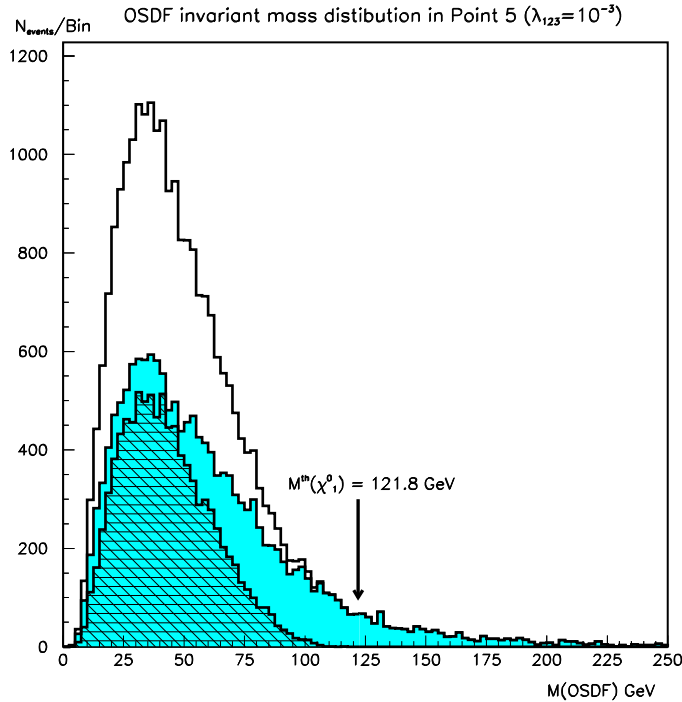


Figure 21: The invariant mass distribution of OSDF leptons in the case of \tilde{R} coupling $\lambda_{123} = 10^{-3}$ for 3 years of LHC run at low luminosity at point 5. *Open histogram* - all events; *shaded histogram* - background and *cross hatched histogram* -signal. The arrow points to the nominal value of $\tilde{\chi}_1^0$ mass. The presence of a τ lepton in the $\tilde{\chi}_1^0$ decay will spoil the endpoint at the mass of $\tilde{\chi}_1^0$.

Reconstruction of $\tilde{\chi}_2^0 \rightarrow \tilde{l}_R^\pm + l^\mp \rightarrow \tilde{\chi}_1^0 + l^\mp + l^\pm$ ($\tilde{\chi}_1^0 \rightarrow \nu_{e(\mu)} + \mu^\pm(e^\pm) + \tau^\pm$) chain

The decay of the $\tilde{\chi}_2^0$ produces in this case at least three isolated leptons. With these leptons one can form pairs of opposite sign (OS) and different flavors (DF) - typical for $\tilde{\chi}_1^0$ decay, or of the same flavor (SF) - typical for $\tilde{\chi}_2^0$. As one mentioned before, $\tilde{\chi}_2^0$ will produce firstly an OSSF pair of leptons through a double 2-body decay and in a second stage, $\tilde{\chi}_1^0$ will produce again one or two leptons. In the conserved R parity case one has used the OSSF combinations. Typically, the lepton associated with \tilde{l}_R has a higher p_t than the lepton associated with $\tilde{\chi}_1^0$ as it can be seen from Fig.22. In these conditions, it is useful to impose, beyond the usual cuts (i.e. lepton multiplicity, E_t^{miss} , etc), a minimal difference

between the p_t of the two leptons taken in the OSSF pairs. To decrease the number of bad combinations with leptons coming from the subsequent τ decay, one increases slightly the p_t^{min} cut on leptons. The OSSF leptons, coming from different decays, are less correlated therefore we relax the cut in angle between them. To eliminate the events with $\tilde{\chi}_2^0 \rightarrow \tilde{\chi}_1^0 + h^0$ we demand furthermore that no h^0 has to be reconstructed in the event.

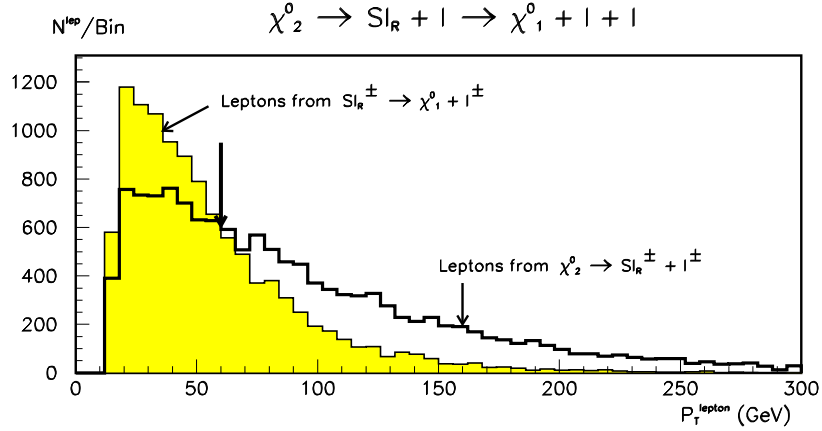


Figure 22: The p_t distributions of the leptons associated with \tilde{l}_R or $\tilde{\chi}_1^0$ in the $\tilde{\chi}_2^0$ decay for 3 years of LHC run at low luminosity at point 5.

In Fig.23, are presented the invariant mass distributions of OSSF lepton pairs, where the events were selected using the following criteria:

- (i) $N_l \geq 4$,
- (ii) $p_t^l \geq 15$ GeV , $\cos(\alpha_{l^\pm l^\mp}) \geq 0$,
- (iii) $E_t^{miss} \geq 50$ GeV,
- (iv) $\Delta p_t^l = |p_t^{l_1} - p_t^{l_2}| \geq 60$ GeV,
- (v) No bb pair with invariant mass in $(m_{h^0} - 15, m_{h^0} + 15)$ GeV.

The huge background comes from the bad combinations with the the leptons produced in the $\tilde{\chi}_1^0$ decays. Since the $\tilde{\chi}_2^0$ decays into the OSSF lepton pair via two 2-body decays, the observed endpoint in the OSSF distribution is determined by the relation of Eq.(15) between $m_{\tilde{\chi}_2^0}$, $m_{\tilde{l}_R}$ and $m_{\tilde{\chi}_1^0}$. After the fit of the Maxwellian background and subtraction, the value of the endpoint is estimated as :

$$m_{OSSF}^{meas} = 111.9 \pm 2.5 \text{ GeV} \quad (29)$$

where the error of about 2.5 GeV is dominated by the histogram binning (i.e. statistics).

One can isolate lepton candidates coming from the double 2-body decay of $\tilde{\chi}_2^0$ by a selection around this endpoint. With the remaining leptons one can attempt to form OS lepton pairs and further combining them with the selected OSSF pairs to reconstruct the $\tilde{\chi}_2^0$. Because of the neutrinos (always present) the $\tilde{\chi}_2^0$ reconstruction is not complete and therefore an endpoint will appear in this OSSF+OS lepton invariant mass distribution depending on the $m_{\tilde{\chi}_2^0}$.

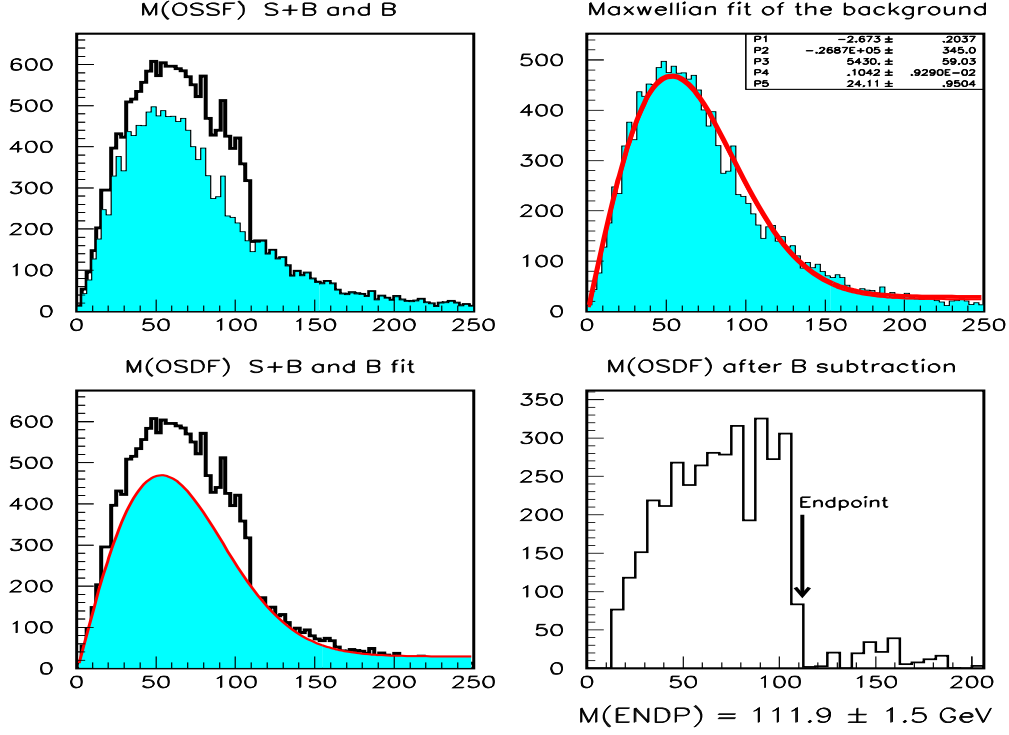


Figure 23: The invariant mass distribution of the OSSF lepton pairs for 3 years of LHC run at low luminosity at point 5.

If one applies the additional cuts to $(i \div v)$:

(vi) $m_{OSSF} \in (m_{OSSF}^{endp} - 25, m_{OSSF}^{endp})$ GeV and rescaled as explained in the introductory part of subsection 5,

(vii) OS pairs constructed with leptons having $p_t^l \geq 10$ GeV, $\Delta p_t^l \geq 20$ GeV and $\cos(\alpha_{OS}) \geq 0$,

(viii) $\cos(\alpha_{OSSF,OS}) \geq 0.85$,

one obtains the distribution represented in Fig.24.

One can observe an endpoint at:

$$m_{\tilde{\chi}_2^0} = 228.2 \pm 5 \text{ GeV} \quad (30)$$

by linear extrapolation of the distribution as is the case for a 5-body final state (see [25]). This endpoint corresponds to the kinematical limit of the $\tilde{\chi}_2^0$ decay, namely to $m_{\tilde{\chi}_2^0}$. The error of the extrapolation is reflected in the large value of the error in $m_{\tilde{\chi}_2^0}$.

Reconstruction of $\tilde{q}_L \rightarrow \tilde{\chi}_2^0 + q$

We observe that at point 5 $m_{\tilde{\chi}_2^0} - m_{\tilde{\chi}_1^0} \approx m^{endp}$ (Eq(15)) which means that the three-momentum of the $\tilde{\chi}_1^0$ is nearly zero in the $\tilde{\chi}_2^0$ restframe. Therefore selecting OSSF lepton pairs near the endpoint of the distribution of Fig.23 one can determine $P_{\tilde{\chi}_2^0}^\mu$ using Eq.(13) with the value of $m_{\tilde{\chi}_2^0}$ from Eq(30). These 4-momenta are then combined with a hard light jet not coming from a reconstructed W or Z^0 . To the criteria $(i \div v)$ one adds the

following :

- (vi - b) $m_{OSSF} \in (m_{OSSF}^{endp} - 30, m_{OSSF}^{endp})$ GeV and rescaled,
- (ix) $p_t^{jet} \geq 400$ GeV and no invariant mass with any other light jet in ± 15 GeV around W ,
- (x) $\cos(\alpha_{jOSSF}) \geq 0$.

The resulting distribution is depicted in Fig.25. By a gaussian fit on the peak one obtains the value:

$$m_{\tilde{q}_L}^{mass} = 683.9 \pm 8.1 \text{ GeV} \quad (31)$$

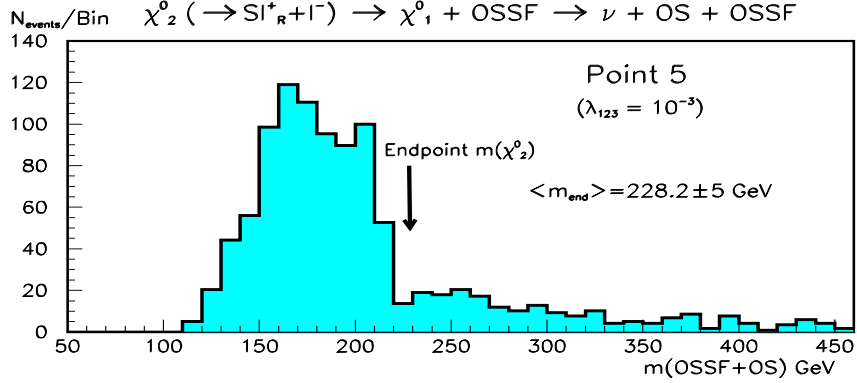


Figure 24: The invariant mass distribution of the OSSF+OS lepton pairs for 3 years of LHC run at low luminosity at point 5. Due to the presence of neutrinos (from $\tilde{\chi}_1^0$ decay) an endpoint depending on $m_{\tilde{\chi}_2^0}$ and $m_{\tilde{\chi}_1^0}$ appears (see text).

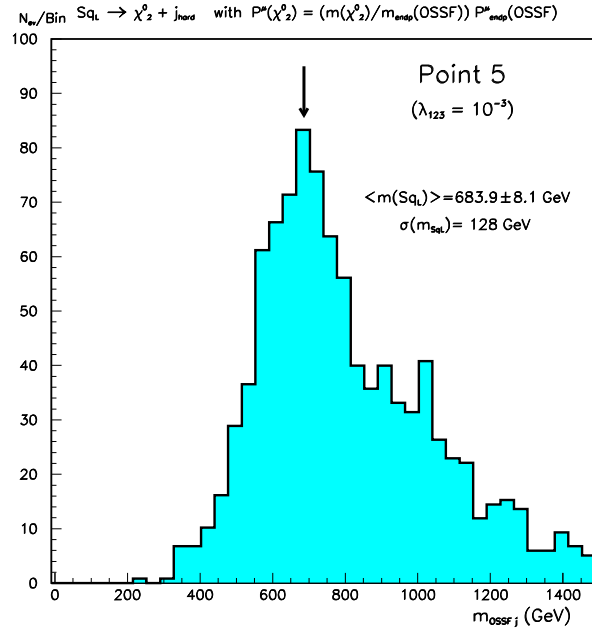


Figure 25: The invariant mass distribution of the (jet OSSF) pairs for 3 years of LHC run at low luminosity at point 5. The arrow points to the nominal value of \tilde{q}_L mass. The mean value is obtained by a local gaussian fit on the main peak.

$m_{\tilde{q}_L}$ can also be determined by combining the (OSSF+OS) pairs selected near the

$m_{\tilde{\chi}_2^0}$ endpoint of Fig.24, whose 4-momenta are approximately equal to $P_{\tilde{\chi}_2^0}^\mu$ according to Eq.(13), with a hard light jet not coming from a reconstructed W or Z^0 . For that one will use the cuts ($i \div ix$) supplemented by:

$$(xi) m_{\tilde{\chi}_2^0} \in (m_{OSSF,OS}^{en\ dp} - 50, m_{OSSF,OS}^{en\ dp}) \text{ GeV},$$

$$(xii) \cos(\alpha_{jOSSF-OS}) \geq 0 .$$

The invariant mass distribution is shown in Fig. 26. One obtains the value:

$$m_{\tilde{q}_L}^{me\ as} = 686.1 \pm 10.3 \text{ GeV} . \quad (32)$$

The agreement between the results of (31) and (32) justifies the procedure that we have applied in obtaining the mass of $\tilde{\chi}_2^0$.

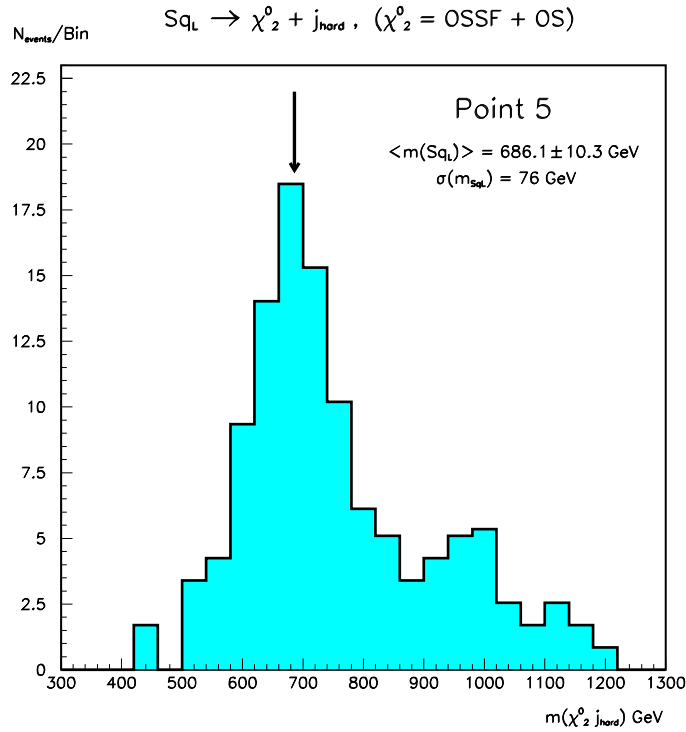


Figure 26: The invariant mass distribution of the (jet OSSF-OS) pairs for 3 years of LHC run at low luminosity at point 5. The arrow points to the nominal value of \tilde{q}_L mass.

Reconstruction of $h^0 \rightarrow b + \bar{b}$

The reconstruction of the h^0 can be carried out almost with the same precision as it was the case of the coupling λ_{122} . However, the applied isolation criteria reject more events due to the finite size of the τ jets as compared to the case of λ_{122} . This can be seen in the $b\bar{b}$ invariant mass distributions which should be independent of the R coupling type. Following the same procedure as in the case λ_{122} , with the selection criteria slightly modified ;

$$(xiii) 15 \text{ GeV} \leq p_t^b \leq 300 \text{ GeV},$$

$$(xiv) \cos(\alpha_{bb}) \geq 0.4 \text{ GeV},$$

one obtains the distribution shown in Fig.27. After the subtraction of the Maxwellian background and the gaussian fit of the peak one gets:

$$m_{h^0}^{meas} = 94.3 \pm 0.17 \text{ GeV} \quad (33)$$

This number does not include the systematic error.

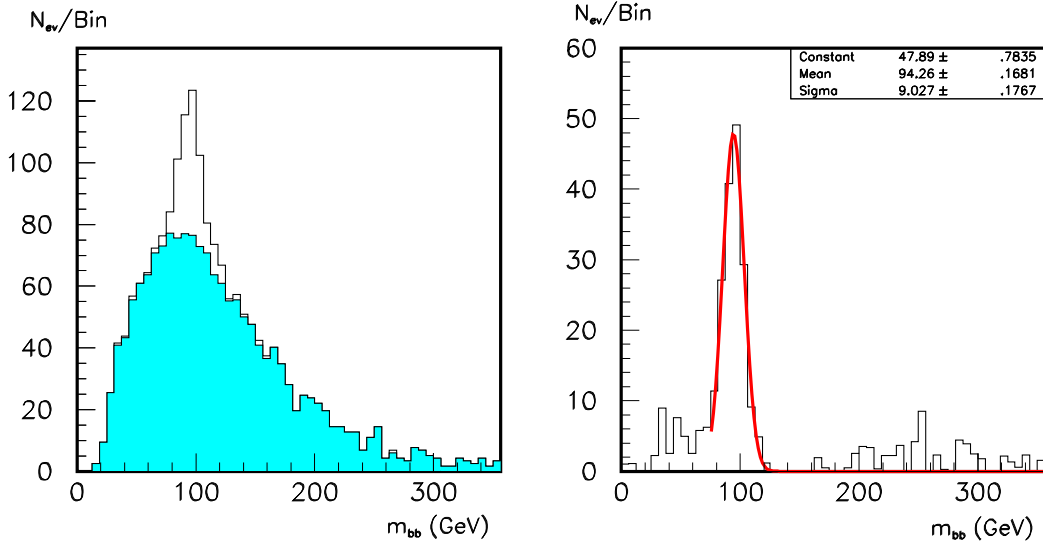


Figure 27: The invariant mass distribution of the (bb) pairs for 3 years of LHC run at low luminosity at point 5.

5.2 The LHC point No3

The salient feature of this point w.r.t. the other two is that the SUGRA parameters m_0 and $m_{1/2}$ are much lower, hence all sparticle masses are lighter and the production cross sections are highly increased. As a consequence we could generate only a fraction of the events one would be able to detect with the ATLAS detector in one year even with low luminosity. In addition, due to the $sign\mu = -1$ and $m_{\tilde{\chi}_2^0} - m_{\tilde{\chi}_1^0} \simeq 52 \text{ GeV}$, the second lightest neutralino decays into OS and SF lepton pairs and not into a Higgs (h^0 , with a mass $\sim 70 \text{ GeV}$). Therefore in this point one cannot determine the Higgs mass. The number of leptons in the final state being higher, the combinatorial background is considerably larger in the channels where the particle reconstruction involves leptons. Furthermore, as we precised before, $\tilde{\chi}_1^0$ can decay (through \tilde{R} λ -type couplings) in lepton pairs of different flavors as well as of same flavors. The consequence is a much more complicated structure in the invariant mass distribution of the OSSF lepton pairs than in the case of conserved R parity.

Another feature of point 3 is that in the decay chain (*) the dominant decay products of the gluino are the \tilde{b}_1 and the b . Since in the decay of the \tilde{b}_1 the gaugino ($\tilde{\chi}_2^0$ or $\tilde{\chi}_1^\pm$) is accompanied again by a b -quark, there is a large number of b -quarks produced in each event.

In the case of conserved R parity [5] the observables which can be used for the determination of the SUGRA parameters are *the functions* $m_{\tilde{g}}(m_{\tilde{\chi}_2^0})$, $m_{\tilde{b}_1}(m_{\tilde{\chi}_2^0})$ and the *difference* $\Delta m_{\tilde{\chi}^0} = m_{\tilde{\chi}_1^0} - m_{\tilde{\chi}_2^0}$ (from the invariant mass distribution of the OS and SF lepton pairs: $\tilde{\chi}_2^0 \rightarrow (l^+l^-) + \tilde{\chi}_1^0$ - see the decay chain (*) and Equ. (12)). In the \mathcal{R} case, one can develop two strategies depending on the λ type coupling :

(1) For λ couplings not producing τ jets in the LSP decays (i.e. λ_{122}) one will *directly* reconstruct the $\tilde{\chi}_1^0$ as in the other LHC points. The consequence of this new information is a better fit of the SUGRA parameters comparing with the R conserved case;

(2) For λ couplings producing τ jets in the LSP decays (i.e. λ_{123}) one returns to the strategy developed in the R conserved case.

As in the LHC points 1 and 5, we will present distinctively the two representative cases: λ_{122} and λ_{123} .

The case $\lambda_{122} \neq 0$

The analysis is focused firstly on the leptons. With these, one can form OS pairs of the same flavor (SF) or different flavors (DF). Due to the facts that:

- $\tilde{\chi}_1^0$ has a significantly higher production rate than the $\tilde{\chi}_2^0$ and
- only $\tilde{\chi}_1^0$ produces $OSDF$ lepton pairs,

the OSDF pairs will tag much better their origine than the OSSF ones. Therefore, in the first stage one will reconstruct the invariant mass distribution of OSDF leptons. This gives the $\tilde{\chi}_1^0$ mass through the same type of endpoint structure as in the other LHC points. The main background in this distribution is combinatorial. One will select OSDF lepton pairs in the neighbourhood of this endpoint. With the remaining leptons (originating with a higher probability from $\tilde{\chi}_2^0$, but also fom $\tilde{\chi}_1^0$) one will form OS lepton pairs. The endpoint in their invariant mass distribution determines $\Delta m_{\tilde{\chi}^0} = m_{\tilde{\chi}_2^0} - m_{\tilde{\chi}_1^0}$. Selecting OS pairs near this latter endpoint and combining them with the $\tilde{\chi}_1^0$ candidates (from the OSDF distribution) one can completely reconstruct $\tilde{\chi}_2^0$. Afterwards, combining $\tilde{\chi}_2^0$ candidates with one and two b jets one will reconstruct \tilde{b}_1 and \tilde{g} .

For this analysis one uses the following global cuts :

- (i) $N_l \geq 4$, and $p_t^{e,\mu} \geq 10$ GeV,
- (ii) $E_t^{miss} \geq 50$ GeV.

Reconstruction of $\tilde{\chi}_1^0 \rightarrow \nu_{e(\mu)} + \mu^\pm(e^\pm) + \mu^\pm$

Using the global cuts (i ÷ ii) and :

- (iii) $\cos(\alpha_{OSDF}) \geq 0.85$,

one obtains the invariant mass distribution of OSDF leptons as in Fig.28, where the background is mainly combinatorial. After the fit of the Maxwellian background, subtraction and the polinomial fit of the resulting endpoint one obtains the $\tilde{\chi}_1^0$ mass :

$$m_{\tilde{\chi}_1^0}^{meas} = 44.8 \pm 0.1 \text{ GeV} \quad (34)$$

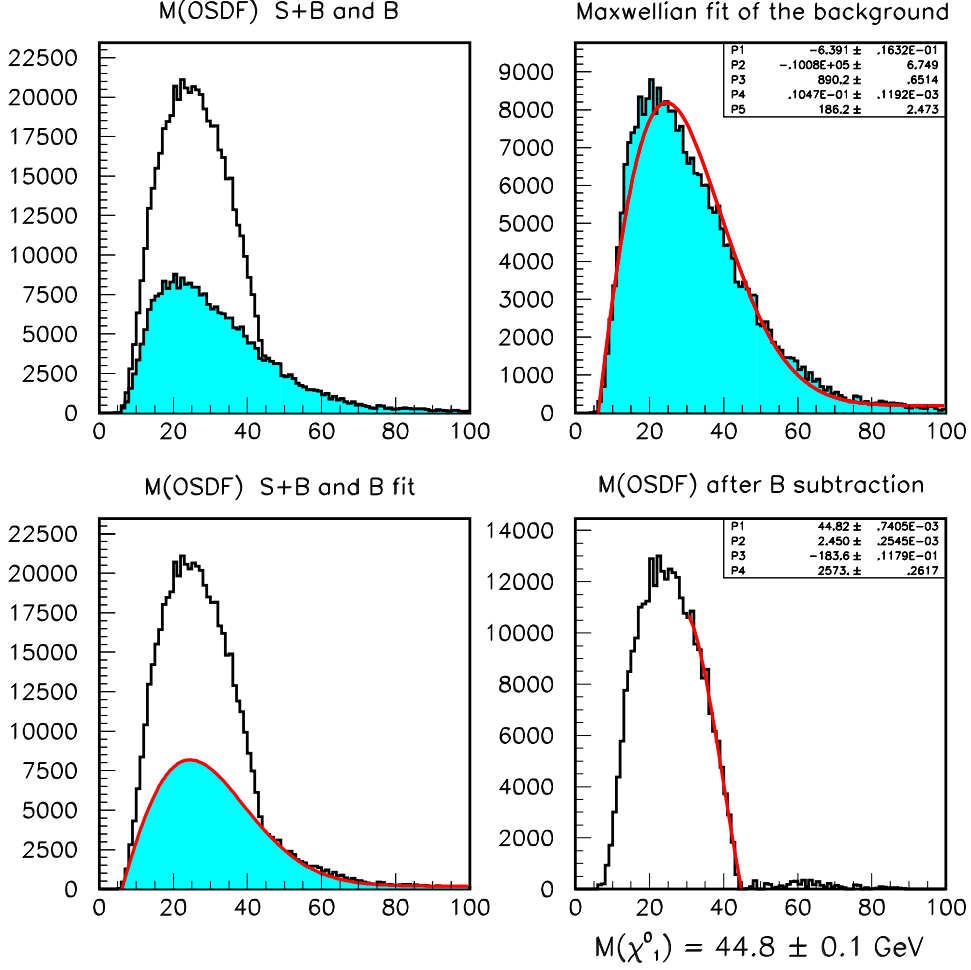


Figure 28: The invariant mass distribution of the OSDF lepton pairs for 1 year of LHC run at low luminosity at point 3 in the case of \tilde{R} coupling $\lambda_{122} = 10^{-3}$.

Reconstruction of $\tilde{\chi}_2^0 \rightarrow \tilde{\chi}_1^0 + \mu^\pm(e^\pm) + \mu^\mp(e^\mp)$

The $\tilde{\chi}_1^0$ candidates are identified by requiring OSDF lepton pairs with :

(iv) $m(OSDF) \in (m_{\tilde{\chi}_1^0}^{meas} - 10, m_{\tilde{\chi}_1^0}^{meas}) \text{ GeV}$,

with rescaled 4-momenta according to Eq.(13). One then selects leptons produced directly from the 3-body decay of $\tilde{\chi}_2^0$ among the remaining OS lepton pairs demanding that the angle between the leptons (α_{OS}) satisfies :

(v) $\cos(\alpha_{OS}) \geq 0.5$.

The invariant mass distribution of these OS pairs (Fig.29) has a complex structure due to the fact that, beside the combinatorial background (Maxwellian type with a long tail) there is also a contribution from the $\tilde{\chi}_1^0$ decay itself (in fact the contribution is 50% of its branching ratio and it has the shape comparable with that of OSDF distribution). Therefore the OS distribution shows a sharp edge at about 52 GeV, corresponding to the mass difference $m_{\tilde{\chi}_2^0} - m_{\tilde{\chi}_1^0}$ and a second one, less pronounced around 45 GeV, corresponding

to the $\tilde{\chi}_1^0$ decay products. The tail beyond 52 GeV is due to the combinatorial background and we have removed it. The polinomial fit of the higher endpoint gives the value:

$$m_{OS}^{meas} = m_{\tilde{\chi}_2^0} - m_{\tilde{\chi}_1^0} = 53.3 \pm 0.6 \text{ GeV} \quad (35)$$

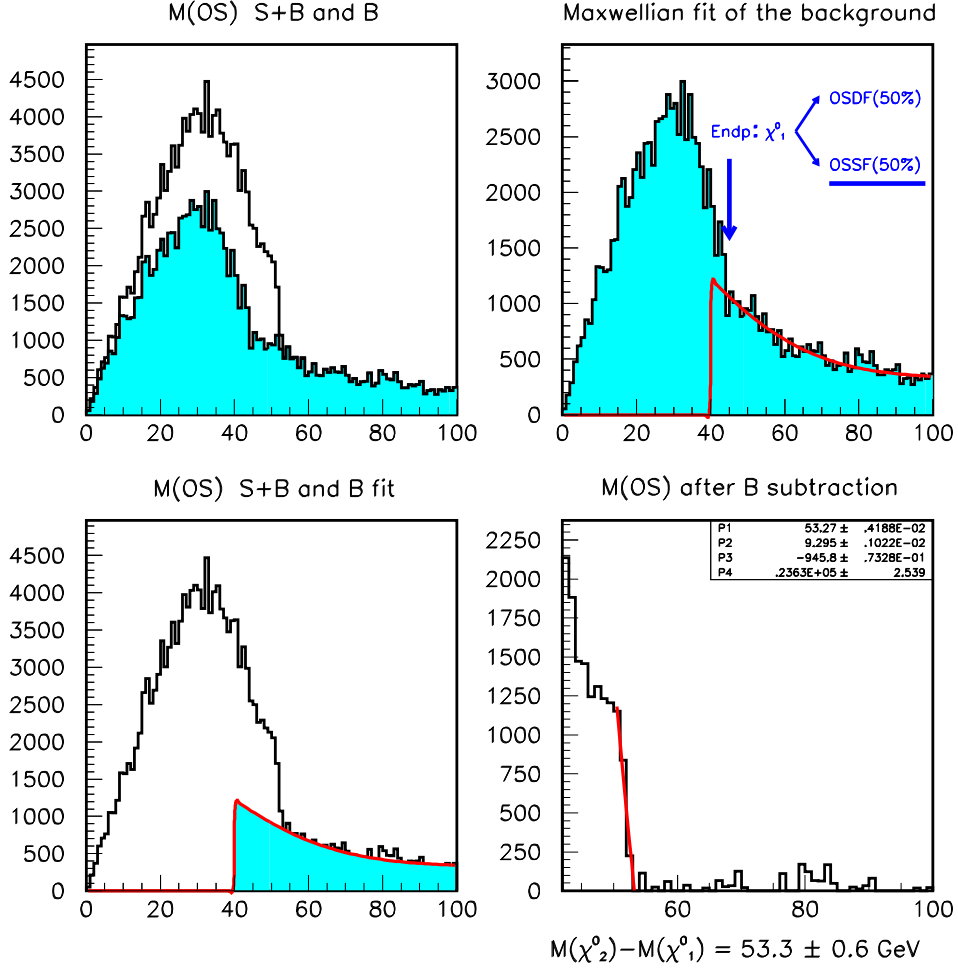


Figure 29: The invariant mass distribution of the remaining OS lepton pairs, after the removal of $\tilde{\chi}_1^0$ candidates. The distributions corresponds to 1 year of LHC run at low luminosity at point 3 in the case of \tilde{R} coupling $\lambda_{122} = 10^{-3}$. For explanations see text.

As a next step we apply the cuts ($i \div v$) and :

$$(vi) m(OS) \in (m_{OS}^{meas} - 10, m_{OS}^{meas}) \text{ GeV},$$

in order to reconstruct the $\tilde{\chi}_2^0$ by combining the OSDF and the remainig OS lepton pairs.

We require that the angle between the two pairs should be small :

$$(vii) \cos(\alpha_{OSDF, OS}) \geq 0.8.$$

The obtained mass distribution is shown in the Fig.30. The gaussian fit around the peak results in the value :

$$m_{\tilde{\chi}_2^0}^{meas} = 96.7 \pm 0.1 \text{ GeV} \quad (36)$$

Out of the three quantities defined by the Eq.(34), (35) and (36) we use two independent ones (Eq.(34) and (36)) , for the determination of the SUGRA parameters.

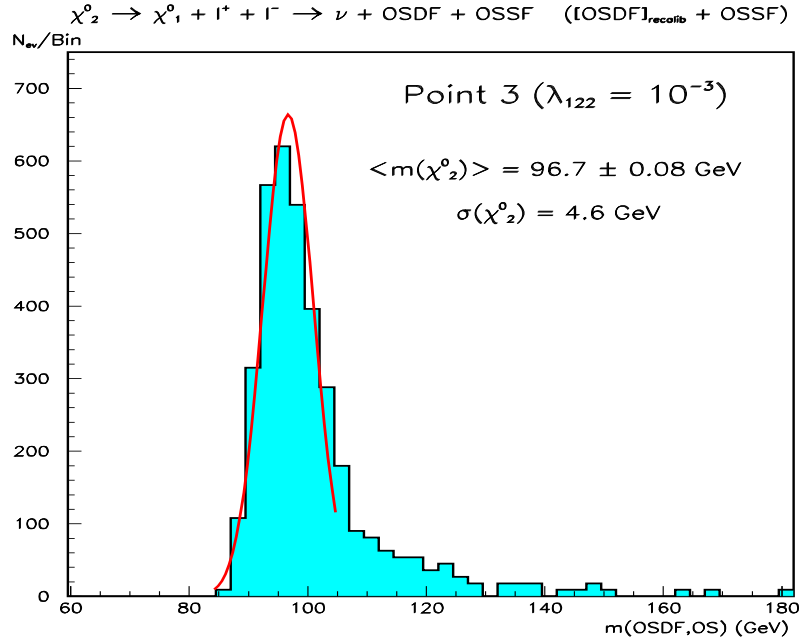


Figure 30: The invariant mass distribution OSDF + OS lepton pairs. The distributions correspond to 1 year of LHC run at low luminosity at point 3. For explanations see text.

Reconstruction of the chain $\tilde{g} \rightarrow \tilde{b}_1 + b \rightarrow \tilde{\chi}_2^0 + b + b$

The configuration of the sparticle mass spectrum (see Table 5) and the decay branching ratios for that point, permit us to make the following remarks on the production of b jets:

(1) practically all b jets originate from the decay chain of \tilde{g} (with a small fraction coming also from \tilde{t}_1 and/or t),

(2) the b jets from the first decay of \tilde{g} are very soft comparing to those produced in the second decay (and associated with $\tilde{\chi}_2^0$), as it can be seen in the Fig.31. Correspondingly we label the b jets as follows :

- (viii) *hard* b jets if : $p_t^b \geq 50 \text{ GeV}$;
- (ix) *soft* b jets if : $10 \text{ GeV} \leq p_t^b \leq 50 \text{ GeV}$.

Selecting $\tilde{\chi}_2^0$ candidates around the $\tilde{\chi}_2^0$ peak from Fig.30 :

- (x) $m(OSDF, OS) \in (m^{peak} - 15, m^{peak} + 15) \text{ GeV}$,

one performs a first reconstruction of the \tilde{g} mass as follows. First of all, one selects pairs of b jets with all b jets passing the cut $p_t \geq 10 \text{ GeV}$ and in each pair we identify the *hard* and the *soft* jet. Next we combine the $\tilde{\chi}_2^0$, b_{hard} and b_{soft} 4-momenta if :

- (xi) $\cos(\alpha_{\tilde{\chi}_2^0 b_{hard}}) \geq 0$, and
- (xii) $\cos(\alpha_{(\tilde{\chi}_2^0 b_{hard}), b_{soft}}) \geq 0.5$.

These cuts are justified by the distributions shown in Fig.32a and 32b.

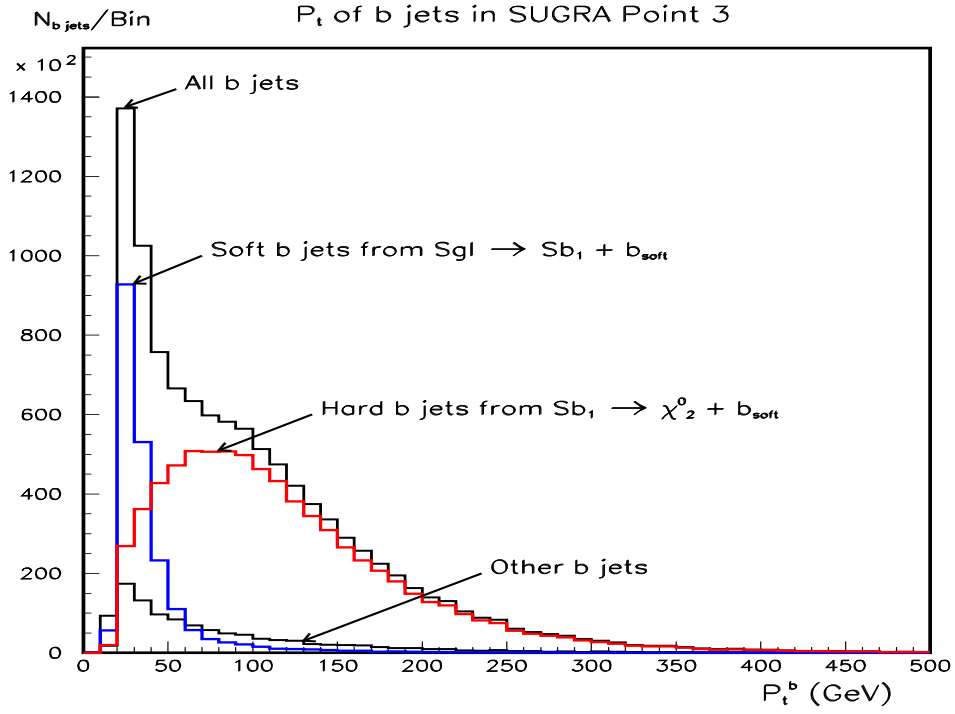


Figure 31: The p_t distribution of b jets in point 3 for 1 year of LHC run at low luminosity after applying the global cuts $N_l \geq 4$, $E_t^{miss} \geq 50$ GeV and $p_t^b \geq 10$ GeV. One can clearly distinguish the b jets from \tilde{g} and from \tilde{b}_1 .

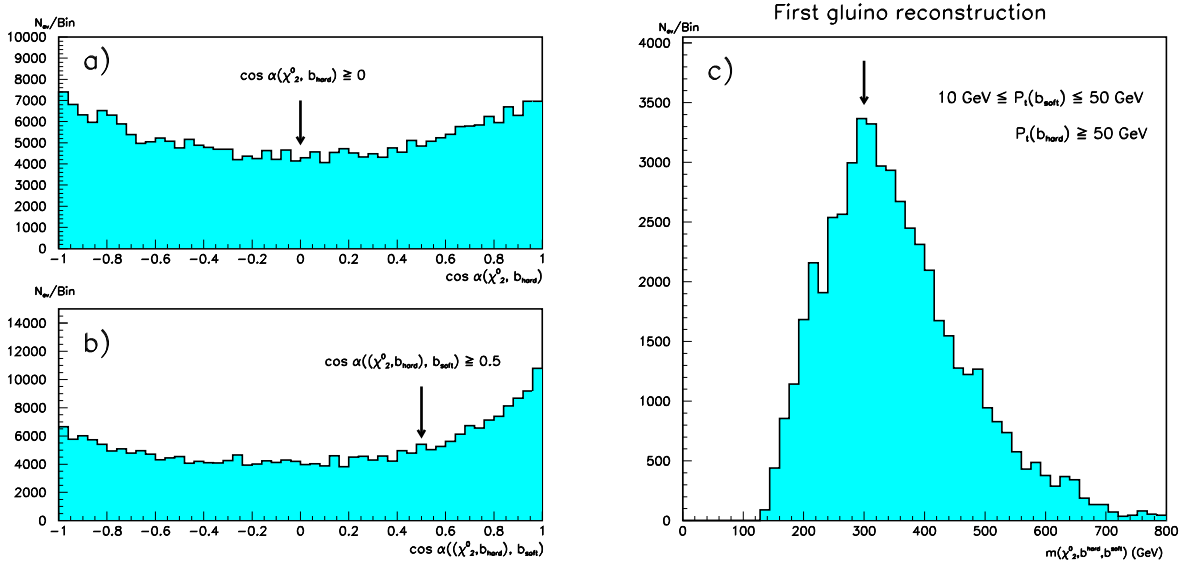


Figure 32: The first reconstruction of the gluino mass in point 3, for \tilde{R} coupling $\lambda_{122} = 10^{-3}$ and after 1 year of LHC run at low luminosity (plot c). Also shown are the angle distributions between the $\tilde{\chi}_2^0$ and the hard b -jets (plot a) and between the $(\tilde{\chi}_2^0, b_{hard})$ pairs and soft b -jets (plot b). For further comments see text.

The resulting mass distribution is represented in Fig.32c. For the \tilde{b}_1 reconstruction, one selects the $\tilde{\chi}_2^0$ candidates according to (x) and the *hard* b jets (see (viii)) around the \tilde{g} peak of the Fig.32c :

(xiii) $m_{\tilde{g}} \in (m^{peak} - 10, m^{peak} + 10)$ GeV, requiring this time

(xiv) $\cos(\alpha_{\tilde{\chi}_2^0 b_{hard}}) \geq 0.5$.

The result is represented in Fig.33. After the gaussian fit around the peak one obtains the value :

$$m_{\tilde{b}_1}^{meas} = 276.6 \pm 0.3 \text{ GeV} \quad (37)$$

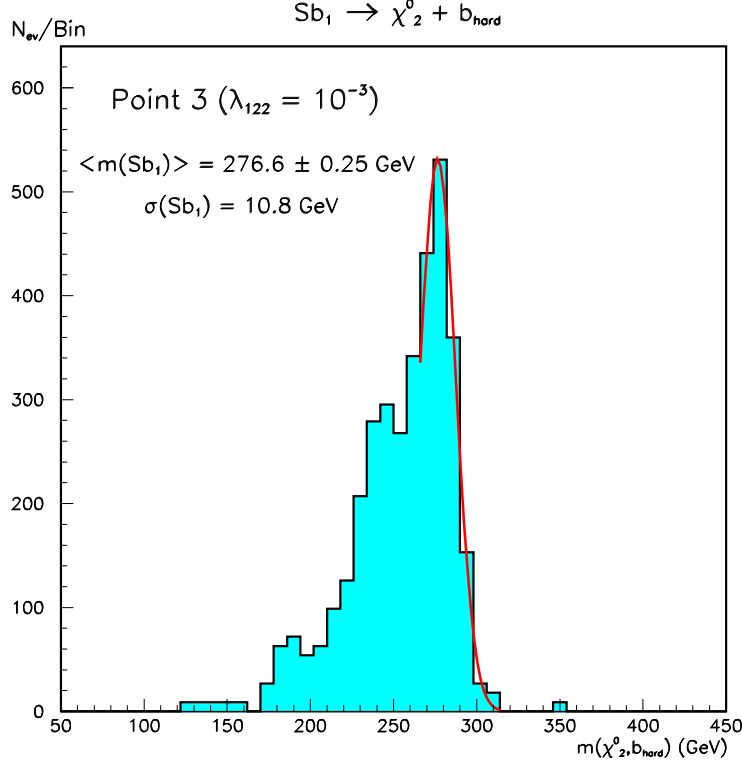


Figure 33: The invariant mass distribution of $\tilde{\chi}_2^0$ and b_{hard} jets. The distribution corresponds to 1 year of LHC run at low luminosity. For the selection criteria see text.

This permits us to refine the reconstruction of the \tilde{g} by tagging it with the \tilde{b}_1 . We combine the $\tilde{\chi}_2^0$ candidates (cut (xi)) with a *hard* b (cut (viii)) requiring an invariant mass within the \tilde{b}_1 mass window:

(xv) $m_{\tilde{\chi}_2^0 b_{hard}} \in (m_{\tilde{b}_1}^{meas} - 10, m_{\tilde{b}_1}^{meas} + 10)$ GeV.

We add subsequently a *soft* b jet with the same angular correlation as (xii) to obtain the final gluino reconstruction shown in the Fig.34. The gaussian fit around the peak gives the measured value :

$$m_{\tilde{g}}^{meas} = 301.1 \pm 0.3 \text{ GeV} . \quad (38)$$

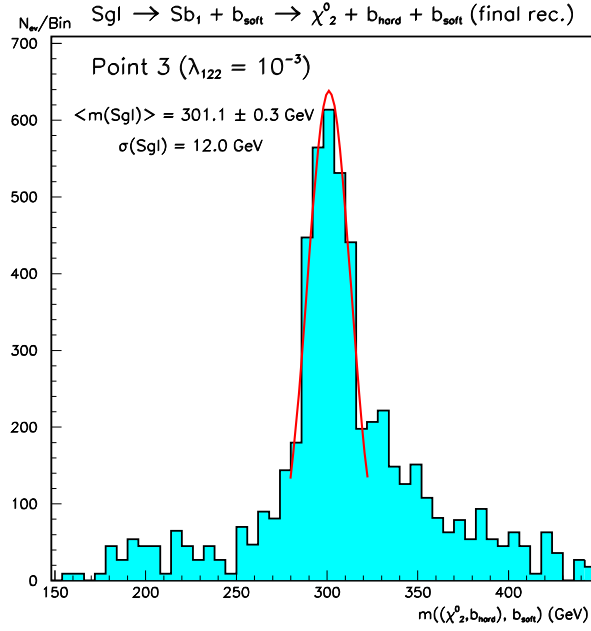


Figure 34: The final reconstruction of the \tilde{g} after having selected the $(\tilde{\chi}_2^0, b_{hard})$ pairs around the reconstructed \tilde{b}_1 mass peak. The distribution corresponds to 1 year of LHC run at low luminosity.

The case $\lambda_{123} \neq 0$

Reconstruction of $\tilde{\chi}_2^0 \rightarrow \tilde{\chi}_1^0 + \mu^\pm(e^\pm) + \mu^\mp(e^\mp)$

Comparing to the case λ_{122} the presence of τ jets in the decay products of $\tilde{\chi}_1^0$ spoils the endpoint structure in the OSDF lepton pair distribution and therefore the direct reconstruction of the $\tilde{\chi}_1^0$. Although the electrons and muons from the τ jets increase the combinatorial background of the OSSF lepton pairs, due the fact that they are softer than those from the 3-body decay of the $\tilde{\chi}_2^0$ they do not spoil the endpoint structure. We select events with the usual cuts ($i \div ii$) and OSSF pairs by requiring :

$$(xvi) \cos(\alpha_{OSSF}) \geq 0.5.$$

After a fit of the Maxwellian tail, subtraction and the fit of the result with a polynomial (see Fig.35), one obtains using Eq.(12) :

$$m_{OSSF}^{meas} = m_{\tilde{\chi}_2^0} - m_{\tilde{\chi}_1^0} = 52.9 \pm 0.01 \text{ GeV} . \quad (39)$$

Reconstruction of the chain $\tilde{g} \rightarrow \tilde{b}_1 + b \rightarrow \tilde{\chi}_2^0 + b + b$

Since the λ couplings do not affect the b jets (if we neglect the difference in the reconstruction and tagging efficiency due to the larger size of a τ jet comparing to a lepton) the classification of b jets in *soft* and *hard* types is done by the same criteria as in the case λ_{122} . The reconstruction of this chain follows the same treatment as in the case λ_{122} with the notable difference that this time one cannot directly reconstruct the $\tilde{\chi}_2^0$. Instead, we have to assume a mass value for the $\tilde{\chi}_2^0$ in order to obtain its 4-momentum

at the endpoint of the OSSF lepton pair mass distribution according to the Eq.(13). We have taken $m_{\tilde{\chi}_2^0} = 97$ GeV.

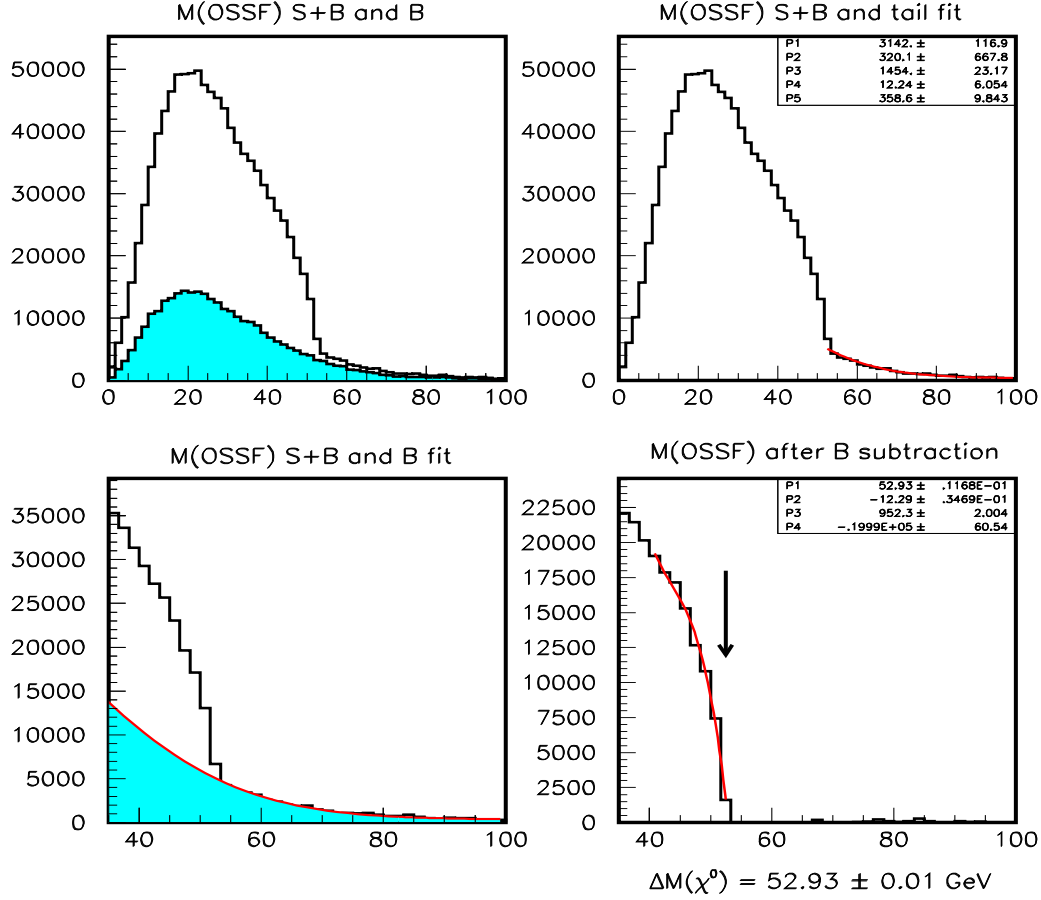


Figure 35: The invariant mass distribution of the OSSF lepton pairs for 1 year of LHC run at low luminosity at point 3 in the case of \mathcal{R} coupling $\lambda_{123} = 10^{-3}$.

The cuts used in this case are the following :

(xi)* $m(OSSF) \in (m_{OSSF}^{endp} - 10, m_{OSSF}^{endp})$ GeV, for the $\tilde{\chi}_2^0$ candidates,
and for the first reconstruction of the gluino :

$$(xii)* \cos(\alpha_{\tilde{\chi}_2^0 b_{hard}}) \geq 0.5,$$

$$(xii)* \cos(\alpha_{\tilde{\chi}_2^0 b_{soft}}) \geq 0.5.$$

The invariant mass distribution of $\tilde{\chi}_2^0 b_{hard} b_{soft}$ pairs is shown in Fig.36. Selecting the *hard* b jets if around the gluino peak :

$$(xiii)* m_{\tilde{g}} \in (m^{peak} - 10, m^{peak} + 10)$$
 GeV and,

$$(xiv)* \cos(\alpha_{\tilde{\chi}_2^0 b_{hard}}) \geq 0.5.$$

one obtains the \tilde{b}_1 mass peak as shown in the Fig.37. The gaussian fit around the peak gives :

$$m_{\tilde{b}_1}^{meas}(97) = 277.5 \pm 0.3 \text{ GeV} \quad (40)$$

The 97 inside the brackets indicates that this value was obtained assuming $m_{\tilde{\chi}_2^0} = 97$ GeV.

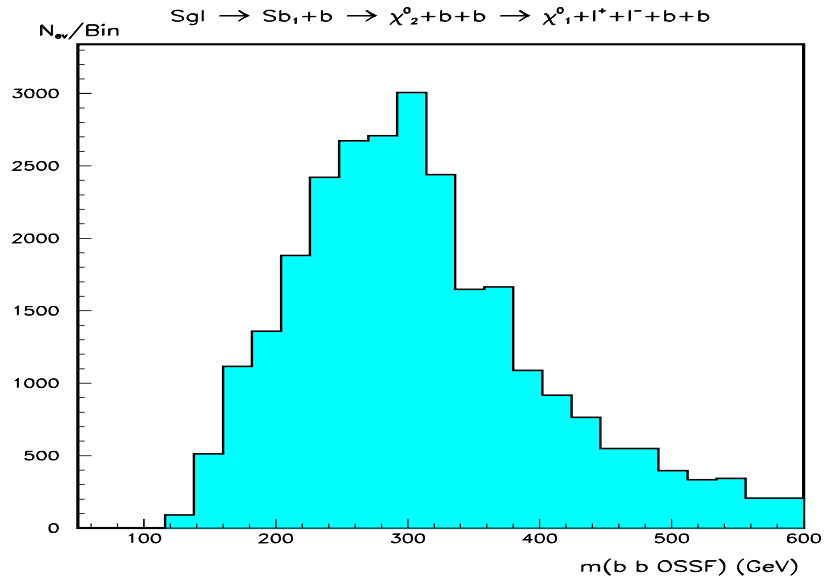


Figure 36: The first reconstruction of the gluino in point 3, for R coupling $\lambda_{123} = 10^{-3}$ and after 1 year of LHC run at low luminosity .

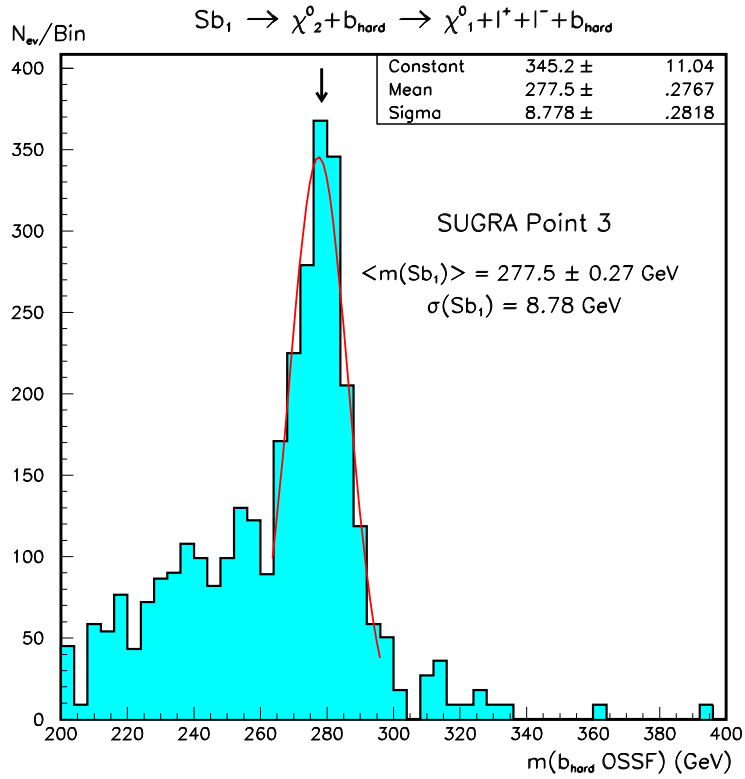


Figure 37: The reconstruction of the \tilde{b}_1 selecting the b jet around the \tilde{g} peak. The distribution corresponds to 1 year of LHC run at low luminosity.

Finally, selecting the *hard* b jets and the OSSF pairs around the \tilde{b}_1 peak :

$$(xv)^* m_{\tilde{\chi}_2^0 b_{hard}} \in (m_{\tilde{b}_1}^{meas} - 10, m_{\tilde{b}_1}^{meas} + 10) \text{ GeV},$$

we combine them with the *soft* b jets with the same angle cuts as above ($(xi)^*$ and $xii)^*$). The resulting mass distribution is shown in the Fig.38. The gaussian fit around the peak gives the measured value :

$$m_{\tilde{g}}^{meas}(97) = 301.1 \pm 0.5 \text{ GeV} . \quad (41)$$

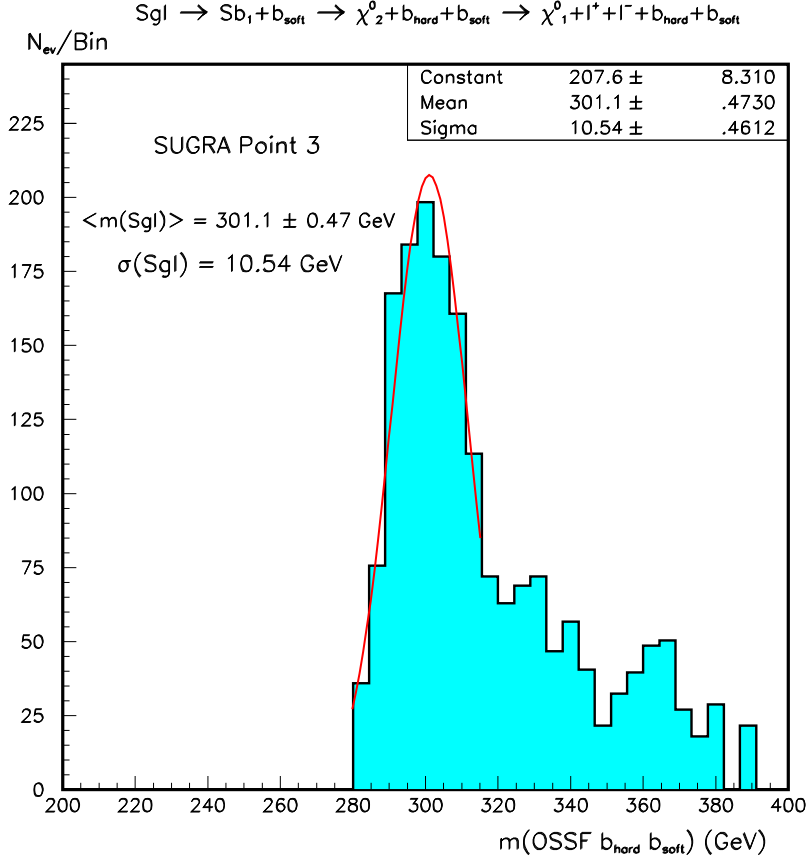


Figure 38: The final reconstruction of the \tilde{g} after having selected the OSSF lepton pairs and *hard* b jets around the \tilde{b}_1 peak. The distribution corresponds to 1 year of LHC run at low luminosity.

We have repeated the above analysis for several different values of $m_{\tilde{\chi}_2^0}$. The result is shown in Fig. 39. Using a linear fit one obtains the following expressions :

$$m_{\tilde{b}_1}^{meas}(m_{\tilde{\chi}_2^0}) = m_{\tilde{b}_1}^{meas}(97) + \theta_{\tilde{b}_1}(m_{\tilde{\chi}_2^0} - 97) \text{ GeV} \quad (42)$$

$$m_{\tilde{g}}^{meas}(m_{\tilde{\chi}_2^0}) = m_{\tilde{g}}^{meas}(97) + \theta_{\tilde{g}}(m_{\tilde{\chi}_2^0} - 97) \text{ GeV} \quad (43)$$

with $\theta_{\tilde{b}_1} = 1.44 \pm 0.54$ and $\theta_{\tilde{g}} = 1.64 \pm 0.52$, respectively.

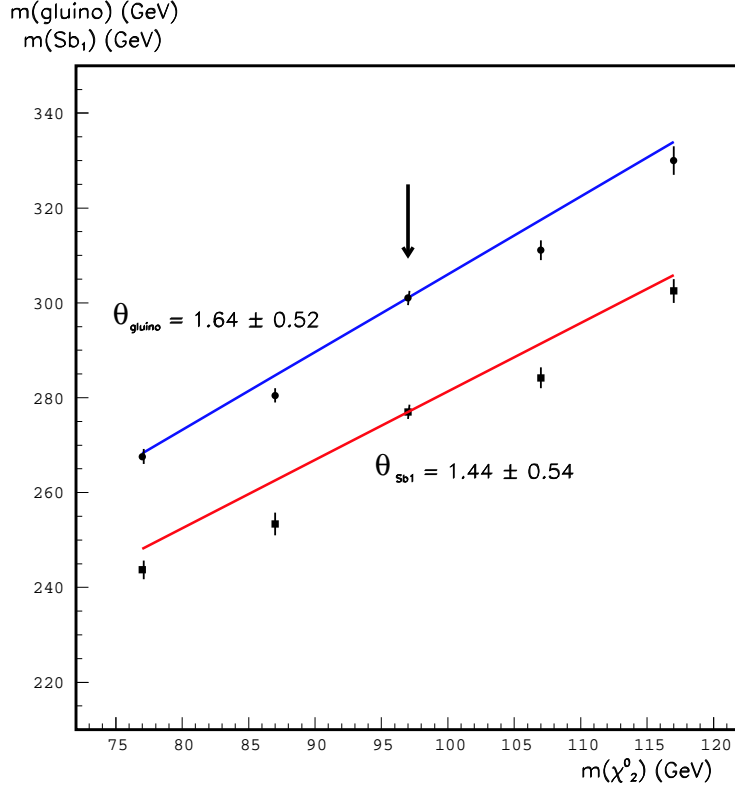


Figure 39: The dependence of $m_{\tilde{b}_1}$ (full squares) and $m_{\tilde{g}}$ (full circles) as functions of $m_{\tilde{\chi}_2^0}$. The arrow points to the nominal value of $m_{\tilde{\chi}_2^0} = 97$ GeV. The factors $\theta_{\tilde{b}_1}$ and $\theta_{\tilde{g}}$ (see text) are extracted by a linear fit.

5.3 Determination of the SUGRA parameters

In subsection 2.2 we have already reviewed the dependence of the sparticle masses as functions of the model parameters m_0 , $m_{1/2}$, A_0 , $\tan\beta$ and $\text{sign}\mu$. Practically all sparticle masses are sensitive to $m_{1/2}$. m_0 drives mainly the sfermion masses. $\text{sign}\mu$ affects the gaugino branching ratios (i.e. $\tilde{\chi}_2^0 \rightarrow \tilde{\chi}_1^0 + l^+ + l^-$ versus $\tilde{\chi}_2^0 \rightarrow \tilde{\chi}_1^0 + h^0$), but also the sparticle mass spectrum. On the other hand, the observables are practically independent of A_0 (c.f. Fig 42 and Table 8). An obvious way to determine the above parameters consists of finding the minimum of :

$$\chi^2(m_0, m_{1/2}, \tan\beta, A_0) = \sum_{\alpha, \beta=1}^{N_{obs}} [O_{\alpha}^{th}(m_0, m_{1/2}, \tan\beta, A_0) - O_{\alpha}^{meas}] \sigma_{\alpha\beta}^{-1} [O_{\beta}^{th}(m_0, m_{1/2}, \tan\beta, A_0) - O_{\beta}^{meas}] \quad (44)$$

where $O_{\alpha}^{th}(m_0, m_{1/2}, \tan\beta, A_0)$ represents the theoretical evolution of the observable α in function of the SUGRA parameters, O_{α}^{meas} is the measured value of the same observable and $\sigma_{\alpha\beta}$ is the covariance matrix ³.

³In general O_{α}^{meas} are not independent, however at the present time we neglect the offdiagonal elements of $\sigma_{\alpha\beta}$.

The minimum of the χ^2 can be found by scanning through the entire parameter space [8]. The overall minimum is practically insensitive to A_0 . The $\text{sign}\mu$ parameter can be determined unambiguously [8]. Once the overall minimum is found one can determine the error on the parameters at the minimum by taking the square root of the diagonal elements of the matrix Δ_{ij} :

$$\Delta_{ij} = \left[\sum_{\alpha,\beta=1}^{N_{obs}} A_{i\alpha}^T (\sigma_{\alpha\beta})^{-1} A_{\beta j} \right]^{-1}, \quad A_{\alpha i} = \frac{\partial O_{\alpha}^{th}}{\partial (p_i)}, \quad p_i \equiv m_0, m_{1/2}, \tan\beta, A_0, \theta_{\tilde{g}}, \theta_{\tilde{b}_1} \quad (45)$$

Table 10 summarizes all the measured values and errors of the chosen observables for all studied cases. For point 3 we have added the h^0 mass determined by an independent measurement ($h^0 \rightarrow \gamma \gamma$) with an estimated error of 1 GeV. As one can see from this Table in most of the cases the models are overconstrained : one disposes of more measured quantities than the number of parameters to be determined. Comparing the measured values of the observables with the theoretical ones (see Table 5) one can see that the errors are slightly overestimated.

$O^{th}(p_i)$ are the theoretical dependencies of the quantities O^{meas} collected in Table 10. However, there is an exception at point 3 (for $\lambda_{123} \neq 0$) where, according to Eqs.(42) and (43) one has :

$$\begin{aligned} O_{\tilde{g}}^{th}(p_i) &= m_{\tilde{g}}(p_i) - \theta_{\tilde{g}}(m_{\tilde{\chi}_2^0}(p_i) - 97), & p_i &= m_0, m_{1/2}, A_0, \tan\beta \\ O_{\tilde{b}_1}^{th}(p_i) &= m_{\tilde{b}_1}(p_i) - \theta_{\tilde{b}_1}(m_{\tilde{\chi}_2^0}(p_i) - 97) \end{aligned} \quad (46)$$

In this case we have to add two more terms to Eq.(44), namely :

$$\chi^2 \longrightarrow \chi^2 + \left(\frac{\theta_{\tilde{g}} - \theta_{\tilde{g}}^m}{\sigma_{\theta_{\tilde{g}}}} \right)^2 + \left(\frac{\theta_{\tilde{b}_1} - \theta_{\tilde{b}_1}^m}{\sigma_{\theta_{\tilde{b}_1}}} \right)^2 \quad (47)$$

and minimize this expression by varying also $\theta_{\tilde{g}}$ and $\theta_{\tilde{b}_1}$. As one can see the errors on $\theta_{\tilde{g}}$ and $\theta_{\tilde{b}_1}$ do not contribute to the errors of the other parameters in the first approximation.

As an example, in the Figs. 40 ÷ 43 we have represented the dependence of the observables on m_0 , $m_{1/2}$, A_0 and $\tan\beta$, respectively, in point 5. Each histogram is fitted with a polynomial in a domain ± 50 GeV - for m_0 , $m_{1/2}$ and A_0 and ± 0.5 - for $\tan\beta$, around the nominal values of point 5. The first derivatives of these functions are used to obtain Δ_{ij} of Eq.(45).

The final results are compiled in the form of relative errors in Table 11, taking A_0 fixed at its nominal value of each point. The obtained precision on the SUGRA parameters are in general higher than in the case of conserved R parity [8]. The reason is that here we were able to determine more observables and usually in a more direct way through the reconstruction of the LSP.

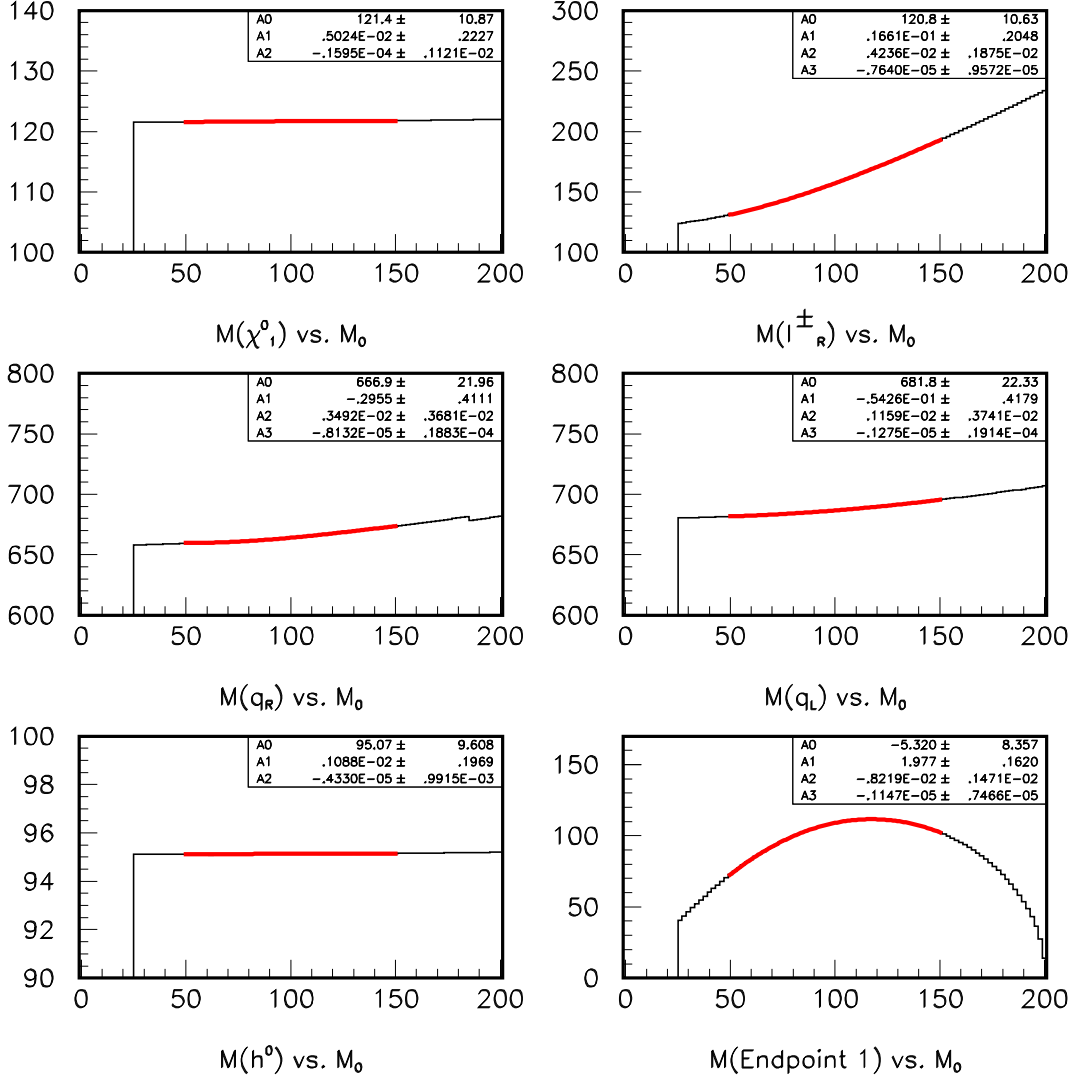


Figure 40: The dependence of $m_{\tilde{\chi}_1^0}$, $m_{\tilde{l}_R^\pm}$, $m_{\tilde{q}_R}$, $m_{\tilde{q}_L}$, $m_{\tilde{h}^0}$ and M_{OSSF}^{end} on m_0 smoothed by a polynomial fit. All other parameters are fixed at those of point 5.

Table 6: The slopes, $\frac{\partial O^{th}}{\partial m_0}$, of the observables at the nominal value of point 5 : $m_0 = 100$ GeV.

$\tilde{\chi}_1^0$	\tilde{l}_R^\pm	\tilde{q}_R	\tilde{q}_L	\tilde{h}^0	M_{OSSF}^{end}
0.001834	0.634610	0.15894	0.13929	0.001954	0.29879

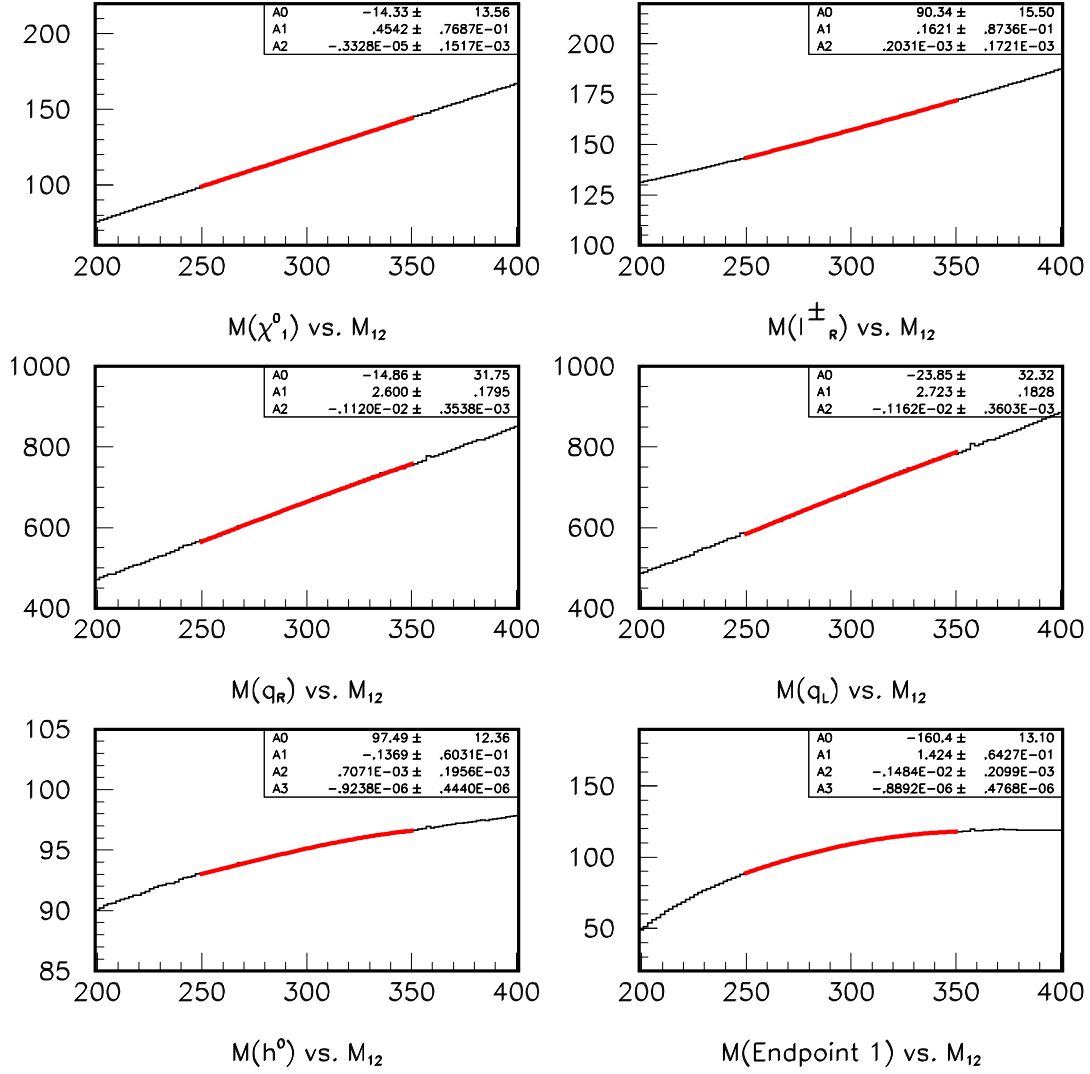


Figure 41: The dependence of $m_{\tilde{\chi}_1^0}$, $m_{\tilde{l}_R^\pm}$, $m_{\tilde{q}_R}$, $m_{\tilde{q}_L}$, $m_{\tilde{h}^0}$ and M_{OSSF}^{end} on $m_{1/2}$ smoothed by a polynomial fit. All other parameters are fixed at those of point 5.

Table 7: The slopes, $\frac{\partial O_\alpha^{th}}{\partial m_{1/2}}$, of the observables at the nominal value of point 5 : $m_{1/2} = 300$ GeV.

$\tilde{\chi}_1^0$	\tilde{l}_R^\pm	\tilde{q}_R	\tilde{q}_L	\tilde{h}^0	M_{OSSF}^{end}
0.452232	0.28396	1.928	2.0258	0.037934	0.293516

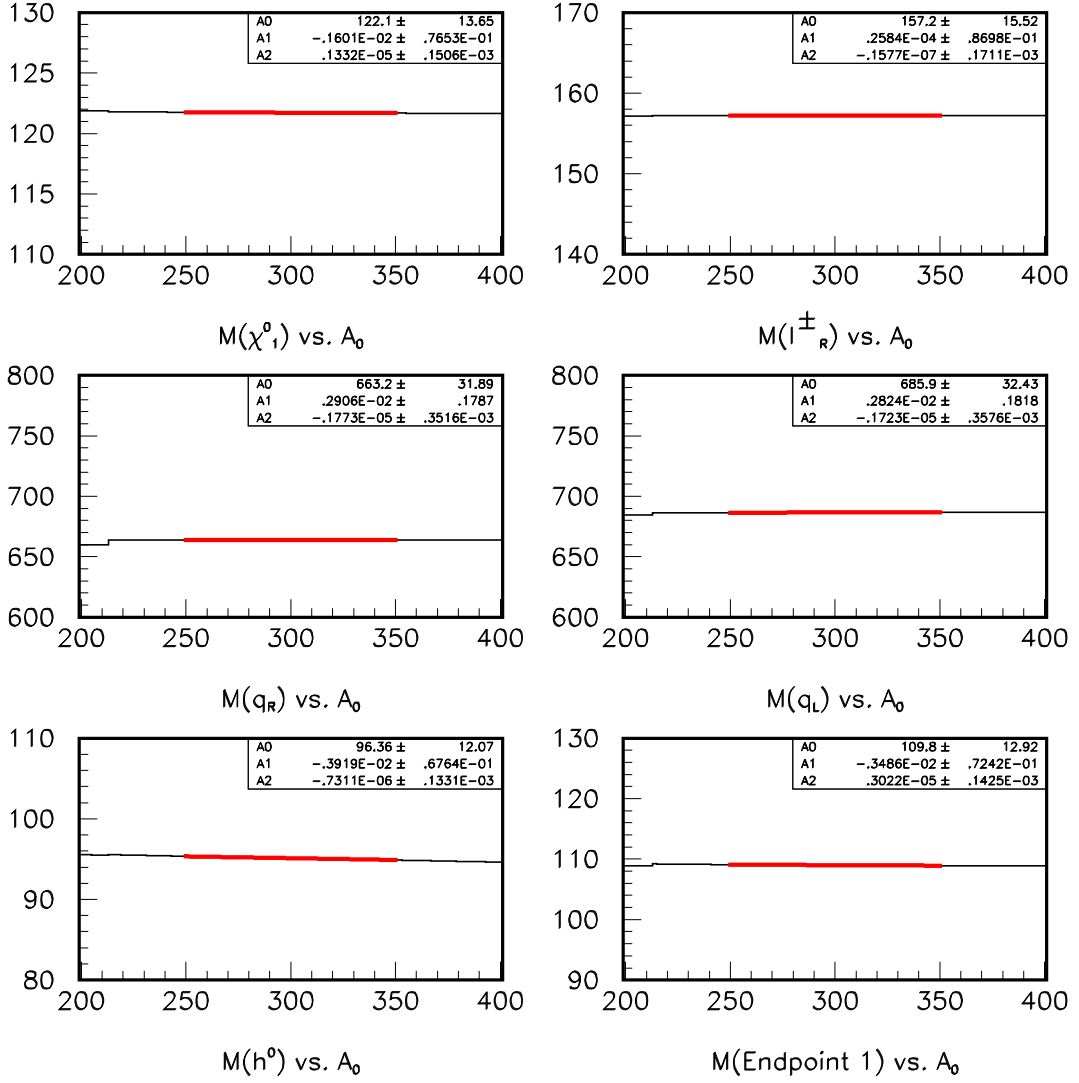


Figure 42: The dependence of $m_{\tilde{\chi}_1^0}$, $m_{l_R^\pm}$, $m_{\tilde{q}_R}$, $m_{\tilde{q}_L}$, m_{h^0} and M_{OSSF}^{end} on A_0 smoothed by a polynomial fit. All other parameters are fixed at those of point 5.

Table 8: The slopes, $\frac{\partial O^{th}}{\partial A_0}$, of the observables at the nominal value of point 5 : $A_0 = 300$ GeV.

$\tilde{\chi}_1^0$	l_R^\pm	\tilde{q}_R	\tilde{q}_L	h^0	M_{OSSF}^{end}
-0.0008018	0.00002584	0.0018422	0.017902	-0.003919	-0.001673

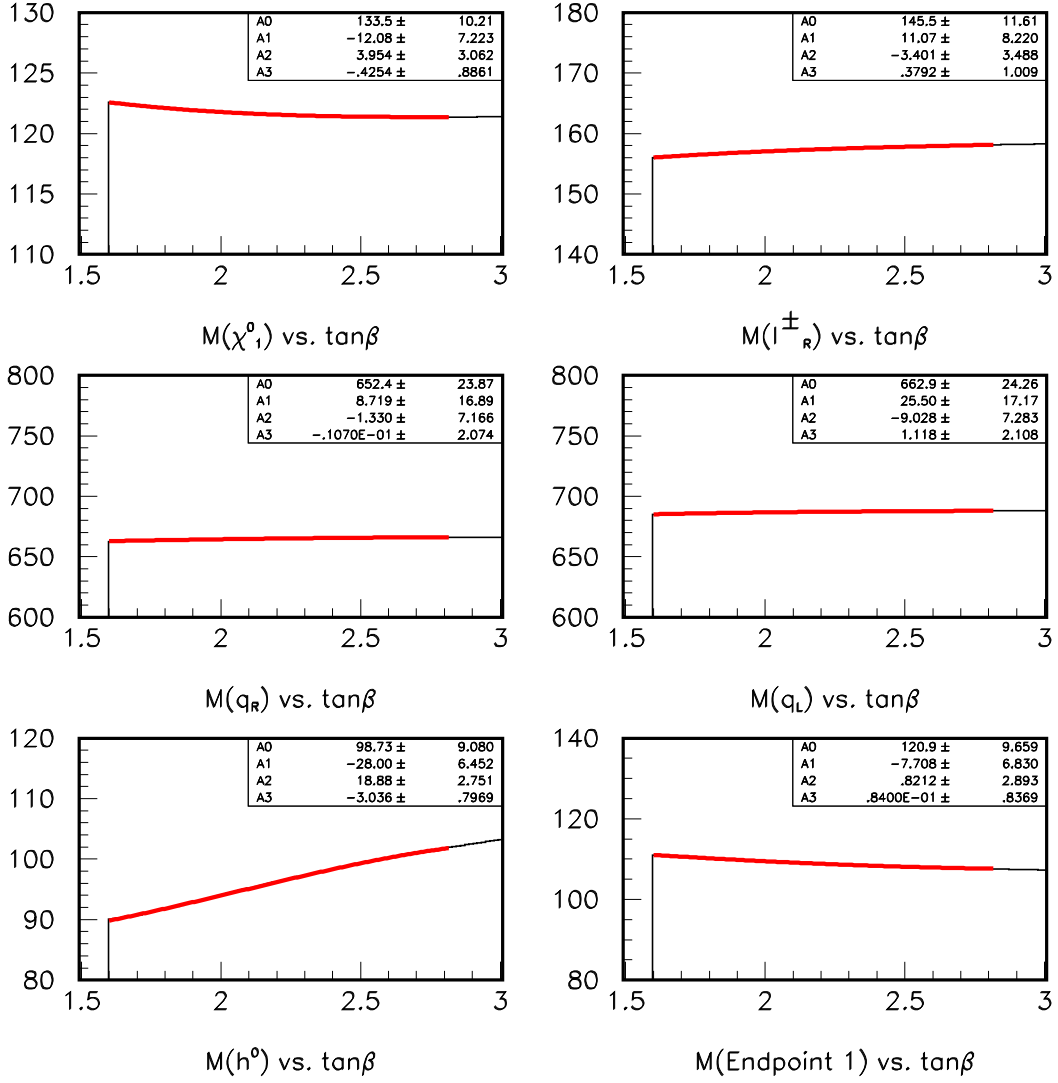


Figure 43: The dependence of $m_{\tilde{\chi}_1^0}$, $m_{\tilde{l}_R^\pm}$, $m_{\tilde{q}_R}$, $m_{\tilde{q}_L}$, $m_{\tilde{h}^0}$ and M_{OSSF}^{end} on $\tan\beta$ smoothed by a polynomial fit. All other parameters are fixed at those of point 5.

Table 9: The slopes, $\frac{\partial O^{\text{th}}}{\partial \tan\beta}$, of the observables at the nominal value of point 5 : $\tan\beta = 2.1$.

$\tilde{\chi}_1^0$	\tilde{l}_R^\pm	\tilde{q}_R	\tilde{q}_L	\tilde{h}^0	M_{OSSF}^{end}
-1.101242	1.802616	2.99144	2.37354	11.1297	-3.14764

Table 10: The measured values of observables in SUGRA points 1, 3 and 5 for each \tilde{R} coupling considered. All the values are in GeV.

$O^{meas} \pm \delta O^{meas}$	Point 1	Point 3		Point 5	
	λ_{122}	λ_{122}	λ_{123}	λ_{122}	λ_{123}
$m_{\tilde{g}} \pm \sigma(m_{\tilde{g}})$		300.9 ± 0.3	301.1 ± 0.5 ³⁾		
$m_{\tilde{q}_R} \pm \sigma(m_{\tilde{q}_R})$	931.7 ± 11.4			662.4 ± 5.1	
$m_{\tilde{q}_L} \pm \sigma(m_{\tilde{q}_L})$				685.2 ± 13.1	686.1 ± 10.3
$m_{\tilde{t}_1} \pm \sigma(m_{\tilde{t}_1})$				503.6 ± 14.3	
$m_{\tilde{b}_1} \pm \sigma(m_{\tilde{b}_1})$		276.6 ± 0.3	277.5 ± 0.3 ³⁾		
$m_{\tilde{t}_R} \pm \sigma(m_{\tilde{t}_R})$				156.8 ± 1.7	
$m_{\tilde{\chi}_1^\pm} \pm \sigma(m_{\tilde{\chi}_1^\pm})$	328.2 ± 5.2			232.2 ± 3.0	
$m_{\tilde{\chi}_2^0} \pm \sigma(m_{\tilde{\chi}_2^0})$	326.2 ± 4.2	97.2 ± 0.1		230.7 ± 2.7	228.2 ± 5.0
$m_{\tilde{\chi}_1^0} \pm \sigma(m_{\tilde{\chi}_1^0})$	169.8 ± 0.1	44.8 ± 0.1		122.6 ± 0.4	
$m_{\tilde{h}^0} \pm \sigma(m_{\tilde{h}^0})$	97.1 ± 0.6	69 ± 1.0 ⁴⁾	69 ± 1.0 ⁴⁾	94.7 ± 0.6	94.3 ± 0.6
$M_{OSSF}^{end\ 1)} \pm \sigma(M_{OSSF}^{end})$					111.9 ± 2.5
$m_{OSSF}^{end\ 2)} \pm \sigma(m_{OSSF}^{end})$		53.3 ± 0.6	52.9 ± 0.1 ³⁾		

$$\begin{aligned}
 1) \ M_{OSSF}^{end} &= m_{\tilde{\chi}_2^0} \sqrt{1 - \left(\frac{m_{\tilde{t}_R}}{m_{\tilde{\chi}_2^0}}\right)^2} \sqrt{1 - \left(\frac{m_{\tilde{\chi}_1^0}}{m_{\tilde{t}_R}}\right)^2} \\
 2) \ m_{OSSF}^{end} &= m_{\tilde{\chi}_2^0} - m_{\tilde{\chi}_1^0} \\
 3) \ \text{Assuming } m_{\tilde{\chi}_2^0} &= 97 \text{ GeV} \\
 4) \ \text{From other measurements } (h^0 \rightarrow \gamma \gamma)
 \end{aligned}$$

Table 11: The relative errors on m_0 , $m_{1/2}$ and $\tan\beta$ in SUGRA points 1, 3 and 5 for each \tilde{R} coupling considered.

Relative errors on the SUGRA parameters	Point 1	Point 3				Point 5	
	λ_{122}	λ_{122}	λ_{123}	λ_{122}^*	λ_{123}^*	λ_{122}	λ_{123}
$\delta m_0/m_0$ (%)	6.9	0.9	1.1	0.8	1.0	2.6	9.6
$\delta m_{1/2}/m_{1/2}$ (%)	0.1	0.1	0.3	0.1	0.3	0.3	1.3
$\delta \tan\beta/\tan\beta$ (%)	3.0	1.2	1.2	1.0	1.0	2.5	2.5

*) If the measurement of m_{h^0} is taken into account.

6 Conclusions

We have studied the feasibility to detect a SUSY signal by ATLAS in the framework of the SUGRA model and to determine its parameters in the case when R parity is broken in conjunction with lepton number violation: $\lambda \neq 0$. For this purpose we have chosen three representative points in the SUGRA parameter space and two different type of couplings, both having a value 10^{-3} , small enough to concentrate the effect in the LSP decay but large enough not to see displaced vertex in this decay.

Our conclusions are the following:

1. The SUGRA signal is visible in a very large domain of the parameter space, even beyond $m_0 \sim m_{1/2} \sim 1$ TeV.
2. The energy scale of the SUGRA signal can be determined by inclusive measurements like the effective mass (m_{eff}) or the normalised transverse momentum per lepton ($p_t^{l, norm}$).
3. In the case of couplings with absence of a τ among the decay products of the $\tilde{\chi}_1^0$ (e.g. λ_{122}) one can reconstruct the SUSY particles and this reconstruction can be used for a precision determination of the model parameters. The achieved precision turns out to be better than it was the case with conserved R parity. This is because one can reconstruct the LSP from its decay products. At the low energy point where the chargino or second lightest neutralino produces additional leptons this determination is slightly handicapped by the combinatorial background and the most complex structure.
4. In the case of LSP decay with a τ particle in the final state the full reconstruction of the LSP, i.e. the determination of its four momentum, is not always possible, however, one can still estimate its mass (except at point 3 - λ_{123}). It allows ones to determine the parameters of the SUGRA model in spite of the large combinatorial background due to the leptonic decay of the LSP. This determination in most of the cases is better or at least comparable in precision with that when R parity is conserved.

Acknowledgements

We would like to thank Daniel Froidevaux for suggesting us to carry out this study, his constant help and encouragement. We had many useful discussions within the ATLAS SUSY working group and would like to express our gratitude to its members, especially to Ian Hinchliffe, Frank Paige and Giacomo Polesello.

References

- [1] For reviews see: H.P.Nilles, Phys. Rep. 111 (1984) 1,
H.E.Haber and G.L.Kane, Phys.Rep. 117 (1985) 75
- [2] L.Alvarez-Gaume, J.Polchinski, and M.B.Wise, Nucl. Phys. B221 (1983) 495,
L.Ibañez, Phys. Lett. 118B (1982) 73,
J.Ellis, D.V.Nanopoulos and K.Tamvakis, Phys. Lett. 121B (1983) 123,
K.Inoue *et al.* Prog. Theor. Phys. 68 (1982) 927,
A.H.Chamseddine, R.Arnouitt and P.Nath, Phys. rev. Lett. 49 (1982) 970.
- [3] I.Hinchliffe, F.E.Paige, G.Polesello, E.Richter-Was, ATLAS-PHYS-No-107

- [4] E.Richter-Was, D.Froidevaux, J.Söderqvist, ATLAS-PHYS-No-108
- [5] I.Hinchliffe, E.Nagy, F.E.Paige, G.Polesello, M.D.Shapiro, J.Söderqvist, W.Yao, ATLAS-PHYS-No-109
- [6] F.Gianotti, ATLAS-PHYS-No-110
- [7] G.Polesello, L.Poggioli, E.Richter-Was, J.Söderqvist, ATLAS-PHYS-No-111
- [8] D. Froidevaux, Precision SUSY measurements with ATLAS, LHCC SUSY Workshop, CERN, 30/10/1996, Unpublished
G.Polesello, Overview of SUGRA studies in ATLAS, ATLAS Physics Workshop, Grenoble, 3/04/1998, Unpublished
- [9] For a recent compilation see e.g.: Report of the group on R -parity violation of the SUSY GdR, hep-ph/9810232, 2 Oct 1998, and references therein
- [10] G.Farrar and P.Fayet, Phys. Lett. B76 (1978) 575
- [11] See e.g.: Physics at LEP2, Vol. I. p. 493 and references therein
- [12] See e.g.: K.Maki and S.Orito, hep-ph/9706382
- [13] A.Mirea, The RPV_ISAJET program, to be published as ATLAS Note
- [14] F.Paige and S.Protopopescu, in it Supercollider Physics, p. 41, ed. D.Soper (World Scientific, 1986)
H.Bauer, F.Paige, S.Protopopescu and X.Tata, in it Proceedings of the Workshop of Physics at Current Accelerators and Supercolliders, ed. J.Hewett, A.White and D.Zeppenfeld, (Argonne National laboratory, 1993)
- [15] E.Richter-Was, D.Froidevaux, L.Poggioli, ATLAS Internal Note Phys-No-79, 1996
- [16] J.Söderqvist, Thesis at the Royal Institute of Technology (KTH), Stockholm, Sweden
- [17] Report of the group on R -parity violation of the SUSY GdR, hep-ph/9810232, 2 Oct 1998
- [18] S.Katsanevas, P.Morawitz, ic/hep/97-5
<http://lyohp5.in2p3.fr//delphi/ktsan/susygen.html>
- [19] T.Sjöstrand, Comput. Commun. 82 (1994) 74
- [20] GEANT Detector Description and Simulation Tool, CERN Program Library Q123
- [21] ATLAS Technical Proposal, CERN/LHCC/94-43, LHCC/P2, 15 December 1994
- [22] PAW - Physics Analysis Workstation, CERN Program Library Q121
- [23] ATLAS Collaboration, ATLAS Inner Detector, TDR.CERN/LHC/97-16, ATLAS TDR 4, 30 April 1997
- [24] P.McNamara, Standard Model Higgs at LEP, talk at ICHEP 1998 Vancouver, Canada
K.Desch, Non Standard Model Higgs at LEP, talk at ICHEP 1998 Vancouver, Canada
- [25] I. Hinchliffe and F.E. Paige, LBNL-42401, BNL-HET-98/37.